

# Steel corrosion damage monitoring in reinforced concrete structures with the acoustic emission technique: a review.

Els Verstrynge<sup>1</sup>, Charlotte Van Steen<sup>1</sup>, Eline Vandecruys<sup>1</sup>, Martine Wevers<sup>2</sup>

<sup>1</sup>*Materials and Constructions division, Civil Engineering Department, KU Leuven, Belgium*

<sup>2</sup>*Materials Performance and Non-destructive Testing group, Materials Engineering Department, KU Leuven, Belgium*

This is a preprint of the paper published as:

Verstrynge, E., Van Steen, C., Vandecruys, E., Wevers, M. (2022). Steel corrosion damage monitoring in reinforced concrete structures with the acoustic emission technique: A review. *Construction And Building Materials*, 349, Art.No. 128732. [doi: 10.1016/j.conbuildmat.2022.128732](https://doi.org/10.1016/j.conbuildmat.2022.128732)

## Abstract

Corrosion is a major issue in construction and infrastructure management, giving rise to high repair costs, safety concerns and structural failures. Especially reinforcement corrosion in concrete structures is a complex issue. As degradation starts internally, visual inspection lacks efficiency in early stages of the corrosion process. Acoustic Emission (AE) monitoring provides major advantages as this technique enables to detect internal damage in an early stage. However, the use of AE monitoring also comes with certain challenges. The aim of this paper is to review appropriate protocols for AE-based reinforced concrete (RC) corrosion monitoring based on an overview of reported lab experiments, highlighting challenges and pitfalls, and to provide a solid basis for extension of the research focus towards on-site AE-based corrosion monitoring in RC structures. Therefore, this paper firstly discusses AE monitoring during (accelerated) corrosion tests, including methods for data analysis and best-practice protocols. Secondly, application of the AE technique for condition assessment of corroded RC elements during load testing is discussed. Thirdly, an overview is presented of reported on-site AE monitoring studies on corroding RC structures. The paper concludes with a discussion and future research challenges, especially towards on-site monitoring of existing RC structures.

## 1. Introduction

There is no doubt that steel corrosion is one of the main challenges in structural engineering, as it affects structural safety and reliability in normal operating conditions and in view of man-made and natural hazards. Especially reinforcement corrosion in concrete structures is a complex issue, as the damage initiates internally in the structure, out of view from inspection, and reinforcement steel corrosion was long not considered a major problem as the steel was thought to be protected by the concrete cover. Yet, the presence of chlorides in marine environments or from de-icing salts, the use of contaminated sand, aggregates or binding water in concrete mixtures, the past use of chlorides as a binding accelerator for concrete [1], or even just the natural carbonation process of concrete cause a breakdown of the protective alkaline environment within the concrete [2]. In addition, flawed design and execution, such as for example water accumulation in incomplete grout filling around post-tensioned strands, may cause accelerated degradation and even structural failure.

The cost of corrosion is very high. The maintenance and related downtime of infrastructure due to steel corrosion and consequential problems take up a large part of the annual budget for civil structures in many countries. For example, the annual direct cost of corrosion for highway bridges in the U.S. is estimated at \$13.6 billion, of which about 40% can be attributed to corrosion in conventional reinforced concrete (RC) [3]. Other examples include the urgent necessary repairs to traffic tunnels in Brussels (2018-2021, Belgium), estimated at over €20 billion for the 2.5 km long Leopold II tunnel alone. In addition, the cost of corrosion-related structural failures goes beyond the mere economic impact. In the collapse of the Polcevera viaduct in Genoa (2018, Italy), which killed 43 people and injured 16, corrosion was an important contributing factor to the collapse, having a devastating effect on the non-robust design with RC stay cables [4]. Also the sudden collapse of an apartment building in Miami (2021, USA), killing 97 people, was attributed to degradation of the RC substructure in a marine environment.

Of the two most cited causes for reinforcement corrosion, being chloride ingress and concrete carbonation, the former is generally most detrimental for an RC structure [2]. While concrete carbonation causes a general reduction of the concrete alkalinity, leading to a distributed micro-cell corrosion process, chloride ingress might induce local acidic conditions and a faster corrosion process with localized macro-cells [5]. At the anodic site of the corrosion cell, steel is dissolved. The iron ions in solution react with hydroxides to eventually form iron oxide, which has an expansive nature as its density is lower than steel, causing internal stresses in the concrete and eventually cracking and spalling. As localized steel section loss, referred to as pitting corrosion, is most detrimental from a structural failure point of view, chloride-induced corrosion receives most attention in research. Of course, both processes may occur combined with mutual acceleration effects [6]. A detailed description of the corrosion process and related electro-chemical reactions can be found in the literature [7].

Regardless of the cause of corrosion initiation, the corrosion process of reinforcement bars (rebars) is generally described as a two-phase process, see Figure 1 [8, 9]. In the initiation phase (phase A), the concrete carbonation front and/or chloride ions progress towards the rebars. At the end of the initiation phase, the critical chloride content or carbonation depth is reached and the corrosion process may start. The second phase, corrosion propagation, is divided into sub-phases in the fib model; before (phase B1) and after (phase B2) concrete surface cracking.

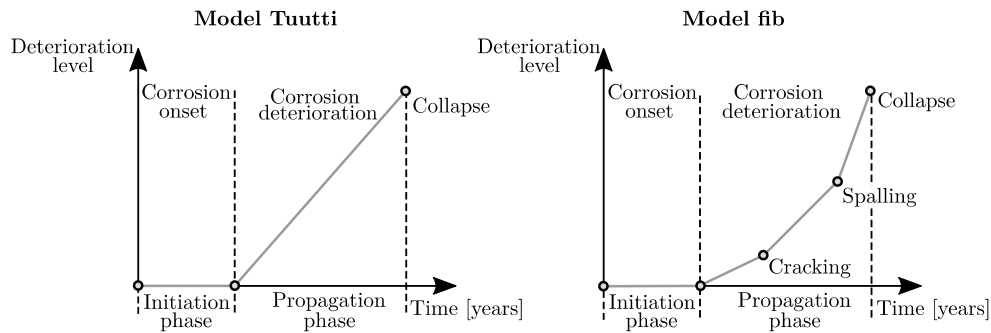


**Figure 1:** Service life models of concrete structures subjected to corrosion of the reinforcement according to (left) Tuutti [9], and (right) fib [8].

New structures are designed not to reach the end of the initiation phase before the end of service life. However, many existing concrete structures are already in the propagation phase, with a substantial part of those structures showing early signs of corrosion damage before their end of service life. Additionally, backlog in maintenance and repair, and lifetime extensions of infrastructure assets are reported in many countries in the past decades [10]. Therefore, the development of monitoring techniques and data-driven management schemes are crucial for safe use of critical concrete infrastructure.

Many monitoring techniques have been developed for corrosion monitoring in concrete structures. Non-destructive electro-chemical techniques, such as half-cell potential and linear polarization resistance measurements, focus on the probability, location, rate and severity of ongoing corrosion processes, yet are often not quantitative and results depend on the measurement conditions and materials involved [11-13]. Corrosion sensors that are embedded in the structure rely on the depassivation and subsequent potential difference or current in an embedded corrosion macro-cell [14], corrosion-induced metal loss to be detected by electromagnetic interference, or alternatively, by wavelength or light intensity shifts in coated fiber optic sensors [15]. Other monitoring techniques, that are referred to as physical techniques, detect corrosion-induced strains and cracking in the concrete. This is done by means of elastic wave techniques such as ultrasonic testing [16-18] and acoustic emission (AE) sensing [19, 20], with electromagnetic waves such as ground penetrating radar (GPR) [21, 22], and by monitoring of strains and cracks on the surface, which can be done for example with fiber optic sensors [15] or visual techniques [20, 23].

Several review papers were published that describe or review techniques for corrosion detection and monitoring in concrete structures. A summary of reported techniques is presented in Table 1, together with their capabilities and limitations. Each technique captures a specific physical parameter (measurand) related to the corrosion process, i.e. related to steel corrosion or concrete cracking, and has a certain active lifetime that is typically (much) shorter than the lifetime of the structure. Therefore, none of them can efficiently be used during the whole lifetime of the monitored asset, and a combination of several techniques into a sensor network is generally considered to be the most robust approach [24].

**Table 1:** Overview of techniques for detection and monitoring of rebar corrosion, based on an analysis of literature references and review papers [20, 24-27]. Techniques used (almost exclusively) in lab experiments or for tests on cored samples are indicated with \*.

Technique	Measurand	Periodic Measurements (PM) / Continuous Monitoring (CM)	Sensor position: embedded (E) / on the surface (S) / no contact (NC)	Corrosion phase in which the technique is applied (A, B1, B2)
<b>Electrochemical methods</b>				
Half-cell potential or Open circuit potential (OCP) monitoring	Potential	PM / CM	E / S	B1
Electrochemical impedance spectrum (EIS) method	Impedance and phase angle	PM / CM	E / S	B1
Resistivity method	Resistivity	PM / CM	E / S	A / B1
(Linear) polarization resistance	Corrosion current	PM / CM	E / S	B1
Galvanostatic pulse method (GPM)	Potential resistance	PM / CM	E / S	B1
Electrochemical noise (EN)	Potential and current fluctuations	PM / CM	E / S	B1
Harmonic analysis method (HAM)	Polarization resistance	PM / CM	E / S	B1
Macrocell current	Current	CM	E	A / B1
<b>Optical methods</b>				
*Digital image correlation (DIC)	Strain	CM	NC	B1 / B2
Optical fiber sensor	strain or refractive index	CM	E / S	A / B1 / B2
Crack measurements	Crack length and width	PM	S / NC	B2
<b>Elastic wave methods</b>				
Acoustic emission (AE)	AE parameters	CM	E / S	A / B1 / B2
Ultrasonic pulse velocity (UPV)	Pulse velocity	PM / CM	E / S	B1 / B2
Impact echo (IE)	Wave velocity	PM	S	B1 / B2
<b>Electromagnetic methods</b>				
Pulse-modulation eddy current inspection	Eddy current	PM	S	B1 / B2
Ground Penetrating Radar (GPR)	Electromagnetic wave velocity	PM	S	B1 / B2
Infrared thermography	Radiation power	PM	S	B1 / B2
Hall-effect voltage	Hall-effect voltage	PM	S	B1 / B2
Magnetic flux loss method	Magnetic field curves	PM	S	B1 / B2
<b>Other methods</b>				
*X-ray CT	Image grayscale	PM	NC	B1 / B2
Strain gauges	Strain	CM	S	B1 / B2
*Chloride concentration	chloride content	PM	concrete samples	A / B1 / B2
*Carbonation depth (e.g. fenolftaleine test)	pH value	PM	concrete samples	A / B1 / B2

This paper presents an in-depth literature review and discussion on the AE technique for corrosion monitoring in RC. AE monitoring is included in Table 1 within the category of elastic wave methods, and is often cited as having great potential for RC corrosion monitoring [20, 25, 27], yet many challenges still need to be addressed and an ill-informed use of the technique might lead to erroneous results. Acoustic emissions are ultrasonic, transient elastic waves that are caused by sudden stress redistributions, e.g. originating from the formation of a crack, or by processes that take place, e.g. pitting corrosion. These high-frequency elastic waves propagate to the surface of the material where they are detected by an AE sensor. Typical AE sensors are based on piezoelectric elements and are designed to have high sensitivity

in a narrow frequency band (resonance sensors) or a flat response in a wide frequency band (broadband sensors). AE signals are detected in the ultrasound range (>20 kHz) and are amplified and filtered before being stored by a high-performance acquisition system with a typical acquisition frequency of several megahertz (MHz). A transient AE signal with indication of typical signal features is presented in Figure 2, and Table 2 gives an overview of common AE parameters, their unit, and description. Such signal, captured by an AE sensor, will be referred to as an “AE hit”. Multiple hits recorded by a set of sensors but originating from the same source at the same moment will be called an “AE event”. When a hit is detected by exceedance of the amplitude threshold (= trigger), the first amplitude crossing is registered as the arrival time of the AE hit at a specific sensor. Yet a pre-trigger recording is typically also saved, as this allows for signal-to-noise ratio analysis and more advanced arrival time picking algorithms. For a more detailed description of the AE technique in general, the reader is referred to the relevant literature [19]. In this paper, focus will be on AE monitoring of corrosion-induced damage in RC, although also references to other materials and applications will be made if relevant.

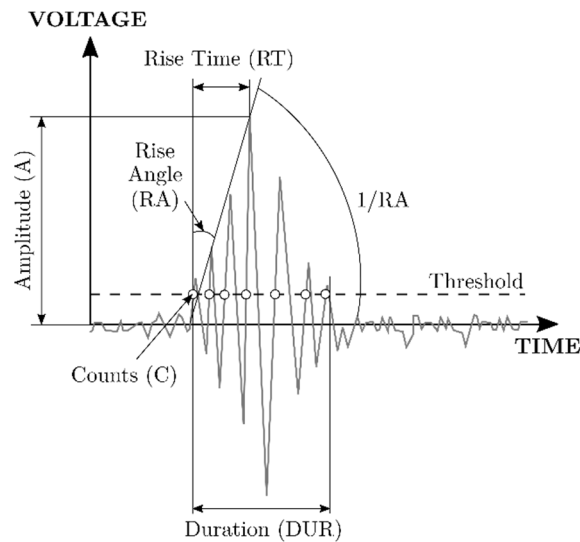


**Figure 2:** Typical AE parameters of a transient AE signal.

**Table 2:** Overview of common AE parameters, based on [28].

Parameter	Unit	Description
Hit	[-]	A signal that exceeds the threshold and is recorded by one sensor
Event	[-]	A number of hits ( $\geq 1$ ) originating from the same source
Peak amplitude (A)	[mV] or [dB]	Maximum voltage of a waveform in the time domain
Rise Time (RT)	[ $\mu$ s]	Time interval between onset time (first threshold crossing) and peak amplitude
Duration (D)	[ $\mu$ s]	Time interval between the first and last crossing of the threshold by a signal
Counts (C)	[-]	Number of times that the signal exceeds the threshold in one polarity
Signal Strength (SS)	[nVs]	Integral of the rectified signal voltage within duration of the signal
Absolute Energy (ABS)	[eu]=[ $10^{-14}$ V <sup>2</sup> s]	Integral of the squared signal voltage within duration of the signal
Rise Angle (RA)	[ms/V]	Rise Time divided by Amplitude, showing the reciprocal of gradient in AE signal
Average Frequency (AF)	[kHz]	Counts divided by Duration. Average frequency is assumed over the entire signal duration
Peak frequency (PF)	[kHz]	Peak amplitude of the signal in the frequency domain
Center frequency (CF)	[kHz]	Center of gravity of the signal in the frequency domain

For rebar corrosion monitoring, the AE technique has several important features that makes it have a vantage point over other techniques. Firstly, it can be used to detect internal damage inside a structural component. As mentioned above, steel corrosion and related concrete cracking are damage processes that occur or initiate inside the concrete. A representation of internal corrosion damage detection with the AE technique is given in Figure 3.

Secondly, the location of the AE source can be determined in one, two or three dimensions depending on the amount of AE sensors that detect the transient signal.

Thirdly, the frequency of AE sensors can be adapted to match the process and material under investigation. This means corrosion-induced micro-cracking can be captured by high-frequency resonance sensors, typically  $> 80$  kHz, while lower-frequency AE sensors (30-80 kHz) can be used for larger scale damage detection. However, it should be noted that the AE technique detects and locates local damage processes, and source-sensor distances are limited by the sensitivity of the sensor within the considered frequency band, the available signal amplifiers and the attenuation of the signal amplitude during wave propagation. The latter is of specific concern in lower-density porous materials [29] and for higher frequency ranges. Thus, AE sensor locations and type need to be chosen with care.

Next, another crucial advantage is the fact that AE signals are produced by the damage process itself, and hence, specific signal features can be related to different AE sources, allowing for AE source identification. This potentially enables to distinguish between signals originating from different damage sources related to corrosion damage: the corrosion process itself and the formation of corrosion pits, wire breakage in pre-stressing strands, concrete cracking and noise sources.

Finally, acoustic emissions are captured at the moment they are produced, or at least within milliseconds, allowing for correlating AE sources and external loads such as the load of a test bench or heavy weight vehicle traffic.

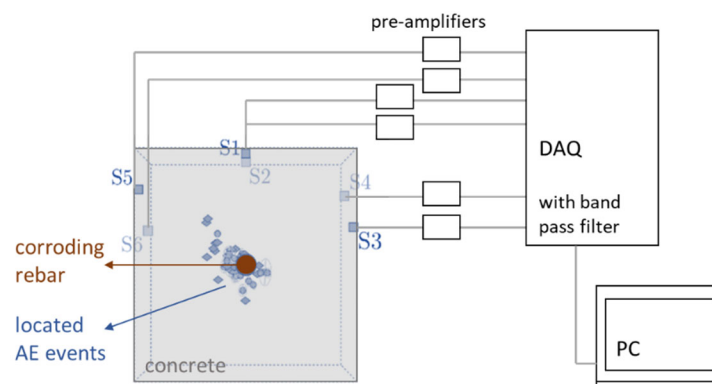


**Figure 3:** Detection and localization of internal corrosion damage, data obtained from [30]. The centrally placed rebar that is shown in front view is subjected to accelerated corrosion, AE sensors (S1-S6) are placed on the concrete cover.

An additional advantage, which AE monitoring has in common with other techniques as well, is its passive nature, which means that it can be applied in operational conditions. However, the technique can also be applied with proof loading to activate damaged zones [31], to monitor crack initiation [32, 33] or to study Kaiser effect under cyclic loading [34, 35]. These methods will be discussed in detail further in the paper.

Challenges in AE monitoring are the need for appropriate data filtering to extract the useful information from the noise, the large datasets resulting from required high acquisition speed to capture the full waveforms in case advanced filtering and analysis is aimed at, and the heterogeneity of RC structures with respect to ultrasonic wave propagation to name a few. These challenges require specific attention during on-site corrosion monitoring in full-scale structures.

In addition to standards regarding AE terminology, calibration, sensors and equipment, see e.g. [28, 36-40], several international standards for AE monitoring in concrete structures have been established:

- ISO 16836: Non-destructive testing—acoustic emission inspection—measurement method for acoustic emission signals in concrete [41]
- ISO 16837: Non-destructive testing—acoustic emission inspection—test method for damage qualification of reinforced concrete beams [34]
- ISO 16838: Non-destructive testing—acoustic emission inspection—test method for classification of active cracks in concrete structures [42]

These ISO standards are based on the work of several RILEM Technical Commissions [43, 44], and were preceded by Japanese standards on AE-based monitoring of concrete structures [45]. ISO 16836 presents general recommendations for AE monitoring in concrete structures, such as relevant frequency bandwidths, calibration and AE parameters to be recorded. ISO 16837 describes a method for qualifying the damage level based on LOAD and CALM ratio, a method that will be briefly discussed further in this paper in view of its relevance for cyclic load tests on corroded RC beams. ISO 16838 presents a procedure to distinguish tensile cracks from other crack types based on the AE signal's rise angle (RA value) and average frequency (AF). This procedure has been applied during corrosion testing as well as for mechanical tests on corroded RC elements, and its performance will be discussed further in this paper. No specific standards or guidelines for AE-based corrosion monitoring in RC structures currently exist.

It is clear from this overview that work is still required to establish protocols for RC corrosion monitoring. Despite the potential, AE-based corrosion monitoring has been mainly applied in lab testing, yet, research is ongoing for on-site monitoring. Therefore, the aim of this paper is to firstly establish appropriate protocols for AE-based RC corrosion monitoring based on an overview of reported lab experiments, highlighting challenges and pitfalls, and then secondly to provide a solid basis for extension of the research focus towards on-site AE-based corrosion monitoring in RC structures.

Therefore, this paper firstly discusses AE-based damage monitoring during accelerated corrosion tests, including methods for data analysis and best-practice protocols as deduced from the literature study. Secondly, application of the AE technique for condition assessment of corroded RC elements during load testing is discussed. Hereafter, an overview is presented of on-site AE monitoring campaigns on corroding RC structures reported in the literature. The paper concludes with a discussion and future research

challenges, focused towards on-site monitoring of existing RC structures, aiming to reduce the current gap between AE-based corrosion monitoring in (accelerated) lab conditions and on-site applications.

## **2. AE for damage monitoring during accelerated corrosion tests**

This section gives an overview on the application of the AE technique for damage monitoring during accelerated corrosion tests of reinforced concrete in a laboratory environment. In section 2.1, an overview of typical setups to initiate corrosion as well as sample sizes and AE sensor types will be presented. Typical AE data filters are summarized in section 2.2. Section 2.3 discusses AE source localization in 1D, 2D, and 3D. As AE analysis may be parameter- or signal-based, section 2.4 gives an elaborate overview on the former and section 2.5 discusses the latter. In section 2.6, clustering of AE signals is presented. Finally, section 2.7 concludes with an overview of best-practice protocols.

### **2.1 Typical setups**

AE monitoring during the corrosion process in a laboratory environment has been investigated on several RC sample sizes ranging from small-scale cylindrical specimens [30, 46-51], to cubes [52], prisms [30, 53-69], and beams [18, 30, 60, 70-75]. Slabs [76-78] and columns [79, 80] have been studied to a lesser extent. Corrosion tests are usually performed under accelerated conditions in order to obtain results within a decent time frame. The corrosion process can be accelerated by means of an imposed current [18, 30, 46, 48, 55, 58], by dry-wet cycles [54, 59, 69, 80], or a combination of both [65, 76, 79]. Few studies focus on natural corrosion processes in which case chlorides are added in the concrete mixture or a salt solution is placed on the concrete surface [49, 53, 74]. To investigate the propagation period, the expansive nature of corrosion can also be mimicked by applying an internal pressure [56, 57]. Depending on the corrosion setup, the presence of water or a salt solution is required. Therefore, samples need to be partially [52, 55, 58, 62] or fully [46, 48, 49] immersed in this (salt) solution. For larger samples, it can be more convenient to place a bottomless tank on top of the sample surface [53, 60, 72, 73]. Most studies focus on only one main corroding longitudinal rebar. Corrosion of multiple rebars [73, 79] and stirrups [30, 71] are less investigated so far. Besides RC, which is of main interest here, pre-stressed concrete (PC) has been investigated as well by several authors [63, 64, 72, 74, 75, 80]. It should be noted that all work referenced in this paragraph concerns tests in which AE monitoring was performed continuously or periodically during corrosion. The sample size and corrosion setup applied have implications for the setup and positioning of the AE sensors.

For AE monitoring of corroding RC components, resonance sensors are most widely used, however, several resonance frequencies were applied by different authors. Resonance frequencies of 30 kHz [18, 46, 47, 61, 70], 60 kHz [53, 55, 58, 63, 64, 67, 72-75, 80], or 150 kHz [48, 49, 54, 56, 57, 59, 68, 69, 77, 79] are mainly reported. In case of signal-based analysis, broadband sensors may be of interest [30, 50, 51, 60, 62, 76, 78]. AE sensors are mostly attached on the concrete surface with vacuum grease or hot melt glue. They can be positioned on one side of the specimen (1D setup), on two sides in a plane (2D) or even in 3D. Depending of the position of the salt solution, AE sensors can be arranged around the zone of interest. Even though AE sensors are attached outside the corrosion zone, they are still able to detect corrosion damage [73, 79, 80]. Of course, the distance between the sensor and corrosion zone is limited

due to attenuation and a larger error is expected on the localization results [19]. Few experiments consider sensors that are attached on the steel rebar [48, 49, 51, 52, 65, 79]. Zheng et al. [79] found that less hits were detected by sensors attached on the rebar than sensors attached on the concrete. Contrary, Li et al. [48] found that the amplitude of signals captured by the sensor on the rebar was higher than the amplitude obtained with the sensor on mortar, and more hits were recorded during the corrosion test for the sensor on the rebar.

Other techniques allow verifying the obtained AE results. A visual inspection of the concrete cover is most straightforward [18, 46, 52, 58, 60, 62, 79]. Also the mass loss of the rebars at the end of the test may be valuable to localize severely damaged zones and pits [62, 64, 66, 72, 75]. During the corrosion process, electrochemical techniques such as half-cell potential, Linear Polarization Resistance, current density, and resistivity allow to assess the onset of corrosion [47, 53, 65, 73, 80]. However, many authors found that the AE technique is able to detect the onset of corrosion earlier than electrochemical techniques [49, 65, 67, 73, 77]. Recently, more advanced inspection techniques such as FBG strain monitoring [48], Scanning Electron Microscope (SEM) [54, 59, 69, 72, 76], and X-ray computed tomography [50] have been applied to verify the AE results from lab tests and to link them with changes in strain due to damage or with the real damage respectively.

## **2.2 Data filtering**

During data acquisition, an amplitude filter is typically applied before identifying and storing transient AE signals. This way, AE hits are distinguished from low-amplitude background noise (see also Figure 2). The advantage is that less unwanted data are stored, thus reducing the necessary data storage. A disadvantage is that low-amplitude signals from the corrosion process or further away sources might be missed. Typical amplitude threshold values applied during corrosion monitoring are 30 dB [51, 53], 40 dB [46-48, 52, 54, 55, 58-60, 62, 67-69, 71-74, 76, 78, 80], 45 dB [18, 70, 79], and 50 dB [57, 61, 64, 75]. It can be seen that a threshold of 40 dB is mostly applied.

Further, AE signals can be filtered during post-processing to eliminate unwanted signals due to noise and wave reflections. Many authors applied a Swansong II filter, which is an amplitude-duration-based filter [58, 63, 67, 72, 73, 75, 79, 80]. The idea behind the filter is that actual AE signals with high amplitudes also have long durations and vice versa. Depending on the amplitude range, a lower and higher boundary rejection limit for the signal duration can be applied. A first drawback of this filter is that the range of rejection limits is determined by subjective visual check of the data, leading to various ranges being reported in the literature. Therefore, Zheng et al. [81] adopted this filter to an amplitude-duration-peak frequency filter. It was found that signals from ambient changes exhibited either a low peak frequency between 0 and 50 kHz or a high peak frequency above 350 kHz. Also Van Steen et al. [60] reported that electromagnetic interference was characterized by a high peak frequency. A second drawback is that sudden burst signals, such as corrosion-induced wire breaks in post-tensioning strands, might be rejected by an amplitude-duration filter. Alternative to the Swansong II filter, filters based on signal-to-noise ratio (SNR) [30, 50, 60] or root-mean-square (RMS) [74] can be applied.

A more advanced noise filtering technique was proposed by Calabrese et al. [82] in which clustering was applied to filter unwanted noisy signals. A combination of different methods such as Principal Component

Analysis (PCA) and k-means was developed. The developed technique was applied during corrosion of a post-tensioned concrete beam. In this study, around 60% of the recorded signals was classified as noise.

### 2.3 Source localization

The localization of corrosion hotspots and cracks is challenging due to the heterogeneous nature of RC. The accuracy of the localization result depends on several parameters such as the sensor layout, the accuracy of the arrival time picking, the velocity model, and the propagation path of the wave. With steel and concrete each with different wave velocities and reflections at interfaces and heterogeneities, the localization result can be severely influenced. Moreover, cracks may have an attenuating effect on the arrival time of the signals [83, 84]. Several localization algorithms are available in the literature [19, 85, 86]. Most algorithms assume a homogeneous velocity and a straight propagation path. In the literature, reported results of localization of corrosion products and cracks are usually obtained with a threshold-based arrival time and a homogeneous wave velocity, e.g. Geiger’s method [87]. More complex algorithms allowing more realistic velocity models and propagation paths are still computationally very demanding [88]. Therefore, the gain in accuracy does not always outweigh the computational time.

Sensors may be arranged in a 1D, 2D, or 3D configuration (see Figure 4), depending on the available amount of sensors and required amount of information, i.e. accuracy of the localization result.

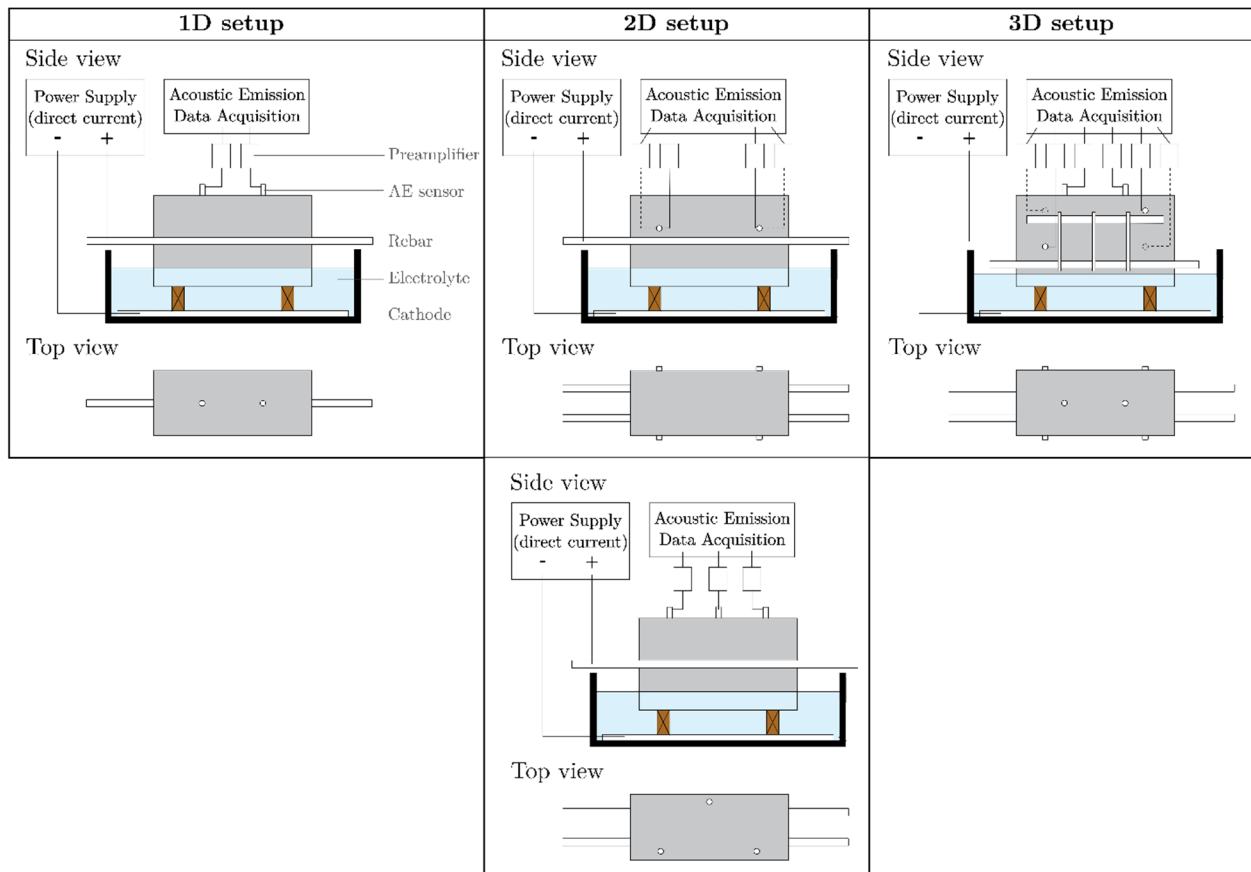


**Figure 4:** Typical 1D, 2D, and 3D setups for AE sensor locations during accelerated corrosion of reinforced concrete.

With a 1D sensor layout, damage can be localized along the length of the rebar and this is typically done for test specimens with one reinforcement bar or prestressing strand [50, 52, 62, 63]. The x-coordinate can for example be plotted against the summed amount of AE events or AE energy of a certain zone [62, 89]. Yu et al. [89] found that the location of AE events is in agreement with the corroding part of the rebar. Moreover, the amount of AE energy was higher for more severely corroded rebars. However, Van Steen et al. [62] found no clear correlation between the amount of AE events or AE energy and rebar mass loss when dividing a more or less uniformly corroding rebar in several zones. This was especially the case for cracked samples. As AE signals are originating from several sources, including concrete cracking, they can therefore not be related to rebar mass loss directly. Mangual et al. [63] reported attenuation due to the presence of cracks leading to less localized events. In non-uniformly corroded beams, a good correlation between the corroding zone and located AE sources was found by Vandecruys et al. [90].

Localization in 2D gives additional information in a second direction [18, 30, 61, 63, 70, 75]. This is particularly interesting in slabs or RC elements with multiple rebars in a same plane. AE events can be localized in the neighborhood of the corroding rebar or local cracks [63, 70, 75]. Results are scattered, but the highest concentration of AE events and AE energy is typically found in the region coinciding with maximum corrosion level and the position of cracks [18, 61, 91].

In case of localization in 3D, the corrosion process can be followed up in more detail as three coordinates are obtained [30, 50, 54, 56, 57, 59, 68, 69, 71]. In this case, the outward progress of cracks from the rebar to the concrete surface, or local corrosion at stirrups can be examined. Kawasaki et al. [54, 59, 69] and Van Steen et al. [30, 50] have reported that initial events were located around the rebar. In a later stage, events are localized outwards towards the concrete surface, following the formed crack paths. It was found that less events were localized in the beginning of the test than in later stages when compared to the total amount of detected events [68]. However, it was reported that AE results enabled the localization of corrosion-induced damage correctly and earlier than a visual inspection [30, 68], as the technique is able to locate internal damage before it can be observed on the surface. A majority of publications focuses on the corrosion process of longitudinal rebars. Li et al. [71] showed that corrosion of stirrups could be localized correctly as well with a 3D setup.

When a threshold-based arrival time is used and AE signals are not filtered, the localization result is scattered. Therefore, it can be challenging to pinpoint the most damaged zones. In a recent paper, Van Steen and Verstrynghe [30] proposed a post-processing protocol combining existing methods to improve the arrival time picking and filtering process for AE-based corrosion monitoring. The arrival time was estimated more correctly by applying the Akaike Information Criterion (AIC). Moreover, noisy signals were removed by an SNR filter and AE events located in 3D. The processing protocol was applied on three sample scales and improved the localization results significantly on all scales. An example of the medium sample scale is presented in Figure 5. In general, the estimation of the arrival time with AIC leads to better source location results, especially when 3D source localization is targeted [59, 68, 69].

In the next sections, typical AE data analysis protocols will be discussed in view of AE-based corrosion monitoring in RC structures.

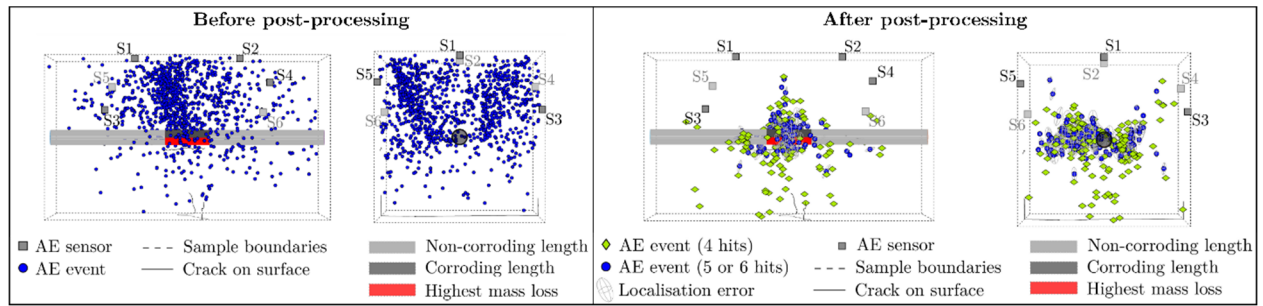


**Figure 5:** Original results (left) and improvement of 3D localization results (right) by a post-processing protocol including more accurate arrival time and filtering, adapted from [30].

## 2.4 Parameter-based analysis of AE data from RC corrosion

Parameter-based analysis makes use of a set of extracted features from the AE signal. It therefore allows an easy and fast analysis of the obtained data [92]. In this section, results obtained by analyzing the cumulative rate of AE events or AE energy, analysis of parameters (such as amplitude, duration, and rise-time), intensity analysis ( $H(t)-S_r$ ), RA-AF analysis, and (i)b-value are discussed in view of their use in corrosion monitoring.

### 2.4.1 Cumulative rate

The cumulative rate of AE events, signal strength (SS), or absolute (ABS) energy versus time is most frequently reported for corrosion tests as it allows analyzing the damage accumulation during the corrosion process. SS is defined as the integrated rectified signal voltage, whereas ABS energy is defined as the integrated squared signal voltage.

Several researchers have investigated cumulative trends of AE hits or AE events to distinguish phases during the corrosion process [18, 54, 59, 60, 64, 65, 67-69, 73]. A transition from one phase to another is typically observed by a sudden increase of the AE events. As such, the onset of corrosion, onset of internal micro-cracking, and the onset of macro-cracking may be obtained. Before cracking, the AE rate is typically linear. After crack initiation, AE trends follow a similar trend as the surface crack width. However, it is reported that the AE rate decreases when severe cracking is observed [79]. Cracks hinder the wave propagation and lead to alternative wave propagation paths. Therefore, sensors may capture less AE hits due to attenuation and reflection.

Alternatively, cumulative SS and ABS energy can be investigated. As for the cumulative AE events, a sudden increase can be noticed between the different phases [18, 46, 50, 55, 58, 60, 63, 64, 67, 73, 79]. Usually the trend is similar as the cumulative AE hits. However, the increase in AE hits and AE energy may not coincide [60]. Di Benedetti et al. [53] and Velez et al. [80] reported that the increase in cumulative SS caused by the onset of corrosion might be masked due to other ongoing processes such as absorption. It may therefore be important to validate the observed sudden increases with other AE parameters or other measurements such as concrete crack measurements and electrochemical techniques. Moreover, these increases may vary between each sample [60, 67]. A general threshold cannot be set and the approach

can thus not be used for quantification of the damage level. Therefore, to distinguish the phases, the entire history needs to be known, which is a drawback of the cumulative approach.

#### 2.4.2 Individual parameter analysis

Besides cumulative events and energy rate, other AE parameters can be investigated such as amplitude, duration, and rise time, refer to Figure 2. It is generally reported that the amplitude increases as the corrosion process progresses [18, 63, 66, 70]. Idrissi and Limam [49] and Mangual et al. [63] also reported that the signal duration and rise time increase over time.

Li et al. [48] distinguished different signal types. Type 1 was assigned to the formation of hydrogen bubbles at the cathode and was characterized by a long duration, high energy, and strong SS. Type 2 was assigned to the generation and movement of corrosion products having a shorter duration, lower energy, and weaker SS. Type 3 had the shortest duration, low energy and SS. This type was assigned to micro-crack development and crack propagation. Again, as reported values for these parameters vary largely between test setups and samples, specific limits cannot be quantified.

#### 2.4.3 RA-AF analysis

Crack classification into tensile cracks (mode I, opening) and shear cracks (mode II, sliding) can be performed by using the AE parameters Average Frequency (AF) (counts divided by duration) and Rise Angle (RA) (rise time divided by amplitude), see also Figure 2. A tensile crack releases most of its energy by longitudinal waves (P-waves) which are characterized by a high AF and low RA value. A shear crack on the other hand, releases most of its energy by transversal waves (S-waves). These S-waves are characterized by a low AF and high RA value [43].

The evolution of RA and AF over time during corrosion has been reported by several authors. Ohtsu and Tomoda [76] reported that RA becomes large and AF low at 40 days of dry-wet cycles indicating that shear cracks were present. Afterwards, RA values were low and AF increased meaning that tensile cracking had initiated (Figure 6 (left)). Similar findings were reported by Leelalerkiet et al. [77]. In contrast, Kawasaki et al. [54] found low RA values in the beginning which later increased, whereas AF decreased over time. However, also during the first stage of the experiment, an increase in RA and a decrease in AF was noticed (Figure 6 (right)). In later work, Ohtsu et al. [68] found no clear trends in the beginning of the test, but RA values decreased and AF increased in a later stage indicating tensile cracking.

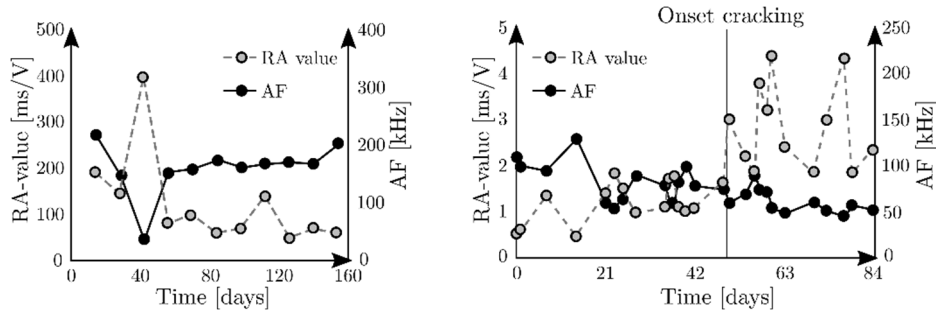


**Figure 6:** Variations in RA values and AF during an accelerated corrosion process: (left) values obtained by Ohtsu and Tomoda [76], and (right) values obtained by Kawasaki et al. [54]. Data are originally reported in [76] and [54] and reproduced here in a similar format for ease of comparison.

Elfergani et al. [61] investigated the RA and AF values of AE events localized in four zones. Two zones with a longitudinal crack, one zone with an inclined crack, and a zone without a crack were selected. A difference could be noticed between the zones. The localized AE events of the zones with a longitudinal crack indicated tensile cracking (high AF, low RA). In the zone with the inclined crack, also an important part indicating shear cracking was observed besides tensile cracking. In the zone without cracks, both tensile and shear cracks were characterized. Moreover, it was mentioned that this result was independent of the distance between source and sensor.

It can be concluded that RA-AF analysis is able to distinguish different crack types when isolated within specific zones of a test specimen, yet when used to analyze AE data obtained as a function of time during the corrosion process, discrepancies are found in the reported results. Hence, the results may be affected by the applied sensor types and filters. It was also reported in the literature that RA-AF values might change as a function of propagation distance, especially in heterogeneous materials [93, 94].

#### 2.4.4 B- value and lb-value

In seismology, events with a large magnitude occur less frequently than events with a small magnitude. A magnitude-frequency relation allows quantifying this and investigate the seismic event. Gutenberg and Richter have proposed an empirical formula which has been modified in order that this principle is applicable to AE data, as acoustic emissions have also been referred to as micro-seismic events [19, 20]. In this way, the scaling of the amplitude distribution of AE signals during the cracking process can be studied. The b-value is the negative gradient of the log-linear AE frequency/magnitude plot and thus represents the slope of the amplitude distribution [95]. Different stages during the cracking process can be observed. It is generally assumed that the b-value is high during early stages of damage and low when macro-cracks begin to localize [96]. Following formula can be applied:

$$\log_{10}N(M) = a - b \left( \frac{A_{dB}}{20} \right) \quad (1)$$

With  $N(M)$  the amount of AE hits or events with a magnitude higher or equal than  $M$ ,  $A_{dB}$  the peak amplitude of the AE events in dB,  $b$  the b-value, and  $a$  an empirical constant.

Leelalerkiet et al. [77] found an increase of the b-value in the beginning of the corrosion test. Later on, the b-value decreased. This may be related to the onset of corrosion and the generation of micro-cracks

during the first stage, and the nucleation of macro-cracks during the second stage. Similar findings were reported by Ohtsu and Tomoda [76]. Abouhussien and Hassan [58] reported many fluctuations of the b-value over time, however, overall, a decreasing trend was observed. The effect of the cover thickness and crack width was investigated as well. A smaller cover thickness and larger crack width led to a lower b-value [58].

An improved b-value, lb-value, was proposed by Shiotani et al. [97]. It is based on the slope of the peak amplitude distribution of AE signals and is defined as:

$$lb = \frac{\log N(\mu - \alpha_1 \sigma) - \log N(\mu - \alpha_2 \sigma)}{(\alpha_1 + \alpha_2) \sigma} \quad (2)$$

With  $\sigma$  the standard deviation of the amplitude distribution,  $\mu$  the mean value of the amplitude distribution, and  $\alpha_1$  and  $\alpha_2$  user-defined constants which represent coefficients of lower and upper limits of the amplitude range to yield a proper straight line [97].

Kawasaki et al. [54, 59] reported two sudden drops in lb-value in the first stage of the corrosion process after which the lb-value increased indicating that micro-cracking had initiated. In the second stage of the experiment, the lb-value decreased and lower lb-values were observed compared to the first stage meaning that larger cracks were formed. When there is more AE activity, sudden drops in lb-value can be seen. Also Ohtsu et al. [68] found a sudden decrease of the lb-value which marked the formation of large tensile cracks.

Although the results found in the literature are rather consistent, this technique is difficult to scale up to larger structures where zones might be in different stages of the corrosion process. In such cases, zonal analysis, localization and comparison with other NDT would help.

#### 2.4.5 Intensity analysis

Intensity analysis uses the signal strength (SS) to generate two parameters called the historic index ( $H(t)$ ) and severity index ( $S_r$ ), as shown in equations 3 and 4 [20, 72, 73, 79].  $H(t)$  reveals sudden variations in the slope of the cumulative SS time history and the increase in severity index  $S_r$  often corresponds to damage. Therefore, both parameters are a measure for the damage severity.

$$H(t) = \frac{N}{N - K} \frac{\sum_{i=K+1}^N S_{oi}}{\sum_{i=1}^N S_{oi}} \quad (3)$$

$$S_r = \sum_{m=1}^J \frac{S_{om}}{J} \quad (4)$$

With N the cumulative number of hits (sorted by time) until time t and  $S_{oi}$  the SS of the  $i^{\text{th}}$  signal.  $S_{om}$  is the SS of the  $m^{\text{th}}$  hit, given that m is sorted in a descending order based on the magnitude of the SS. K and J are constant values that depend on the damage mechanism and type of material under consideration. For concrete, K values are related to N by the relations:  $N \leq 50$ ,  $K=0$ ;  $51 \leq N \leq 200$ ,  $K=N-30$ ;  $201 \leq N \leq 500$ ,  $K=0,85N$ ; and  $N \geq 501$ ,  $K=N-75$  as well as J values for  $N < 50$ ,  $J=0$  and  $N \geq 50$ ,  $J=50$  [67, 72, 98].

As the historic and severity index are related to SS, sudden increases in cumulative SS over time can also be observed in fluctuations of these indices over time. Therefore, these are damage parameters that allow to distinguish different stages, such as onset of corrosion and onset of micro- and macro-cracking, during the corrosion process [53, 67, 75, 79]. Abouhussien and Hassan [58] investigated the influence of the cover depth on the historic and severity index. It was found that both intensity parameters were not significantly affected by the cover depth. However, it is reported that the intensity parameters decrease when sensors are located further away from the corrosion zone [73, 79]. This indicates that the intensity parameters are dependent on the source-sensor distance. Therefore, as was discussed for the cumulative events, SS, and ABS, the magnitudes of the intensity parameters cannot be correlated directly to the corrosion level [73]. Moreover, the amount of hits was reported to be important for an accurate estimation of the corrosion onset [53].

Maximum values of the intensity parameters can be plotted in  $H(t)$ - $S_r$  charts. An example is shown in Figure 7. These charts can be divided in zones and may allow to distinguish the damage level. The bottom left area of the chart is for zones exhibiting negligible damage, whereas the top right area of the chart indicates major damage. However, boundaries between the zones may be dependent on the specific setup. Mangual et al. [63, 75] proposed boundaries based on empirical results. The amount of damage was quantified by half-cell potential measurements and rebar mass loss. The same boundaries were applied by ElBatanouny et al. [72] as a similar concrete mix and the same AE sensors were used. The results agreed with the obtained corrosion level as determined by linear polarization resistance measurements. Also Appalla et al. [74] applied the same boundaries and reported results coincided with the half-cell potential measurements.

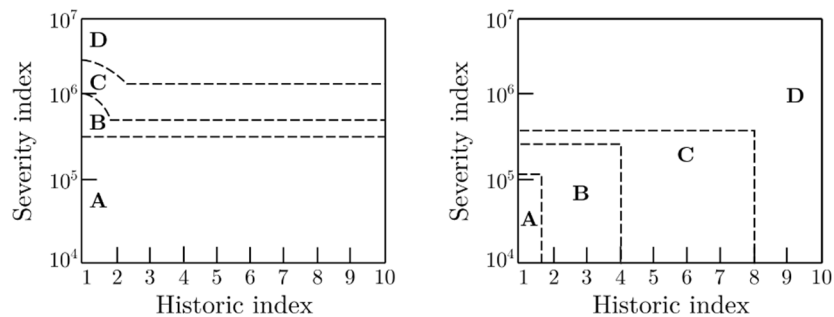


**Figure 7:** Examples of  $H(t)$ - $S_r$  plots with limits according to Mangual et al. [63] (left) and Velez et al. [80] (right), the zones indicate (A) no depassivation, (B) depassivation, (C) cracking, and (D) severe cracking.

Boundaries were adapted by Velez et al. [80] to make the values of  $H(t)$  and  $S_r$  consistent with the levels of corrosion meaning that depassivation values were obtained for non-corroding PC piles and damage values for corroding ones. Abouhussien and Hassan [58] found that the results of the  $H(t)$ - $S_r$  chart showed to be only related to the amount of concrete crack growth and not to other parameters such as corrosion level, cover thickness, and test duration. Yet in a later publication, a good correspondence between the  $H(t)$ - $S_r$  chart and corrosion level was obtained by the same authors [73]. Still, a drawback of the method is that the technique depends on the number of data points and empirically derived constants [53, 80, 98], as well as being affected by the sensor layout and source-sensor distance. As boundary values are difficult to quantify, the full history is required to identify changes in damage level.

## 2.5 Signal-based analysis of AE signals from RC corrosion

An advantage of the AE technique is that the characteristics of an AE signal depend on the source type. Signal-based analysis, which makes use of the entire waveform instead of few parameters describing the signal, could provide more information on the identification and characterization of AE sources. This is especially useful for corrosion in RC, as several types of AE sources such as corrosion and crack initiation are present at the same location in the RC structural component. In this section, frequency analysis and moment tensor analysis are discussed.

### 2.5.1 Frequency analysis

By applying a Fast Fourier Transform (FFT), the AE signal can be converted from the time domain to the frequency domain. The frequency content of the signals can be analyzed by looking at the peak or center frequency. The former is defined as the maximum amplitude of the signal in the frequency domain. The latter is defined as the center of gravity of the signals in the frequency domain.

An initial study was presented by Di Benedetti et al. [53] in which it was found that AE signals generated by breakage of the steel passivation layer have a low frequency between 35 and 50 kHz. However, AE signals generated by active corrosion were difficult to isolate in a specific frequency range. Li et al. [48] reported three groups based on analysis of the peak frequency. All groups were observed from the beginning of the test. Group 1 was characterized by signals with a frequency below 50 kHz, which was assigned to the formation of hydrogen bubbles. Group 2 had signals with a frequency around 110 kHz, whereas group 3 had signals with a frequency higher than 240 kHz. Group 2 was assigned to corrosion and group 3 to concrete cracking after the findings of Yoon et al. [99] who tested corroded RC beams subjected to four point bending tests. Four groups were found by Zheng et al. [79]: (1) below 30 kHz, (2) around 50 kHz, (3) around 150 kHz, and (4) higher than 200 kHz. The groups were respectively assigned to absorption, the formation of hydrogen bubbles, corrosion, and concrete cracking. Reference was made to the work of Li et al. [48] and Yoon et al. [99] to assign the processes.

A dedicated study was performed by Van Steen et al. [60] in which several corroding and non-corroding dummy samples were tested to spatially isolate AE sources. It was observed that frequency ranges of most AE sources overlap and are related to the sensor sensitivity. However, AE signals originating from concrete macro-cracking clearly showed a distinctly lower frequency (Figure 8 (left)). In addition, high-frequency components (> 500 kHz) could be attributed to noise. As frequency ranges of AE signals from corrosion damage overlapped, a more detailed analysis of time-frequency components was performed by means of the continuous wavelet transform. Nonetheless, findings are contradicting the results reported by Li et al. [48] and Zheng et al. [79] where corrosion was assumed to have a higher frequency than concrete cracking. A possible explanation may lie in the use of a different sensor type, i.e. 100-400 kHz broadband sensors by Van Steen et al. [60] versus 150 KHz resonance sensors by Li et al. [48] and Zheng et al. [79]. Therefore, additional tests with a 150 KHz resonance-type AE sensor were executed by Van Steen et al. (Figure 8 (right)). It was concluded that the characteristics of AE signals from processes such as corrosion, absorption and cement hydration are influenced by the sensor sensitivity. Yet also for the resonance sensors, a decrease in frequencies was observed for concrete cracking, confirming the results of the flat

response sensors [60]. Hence, absolute values for AE source characteristics should be approached very carefully.

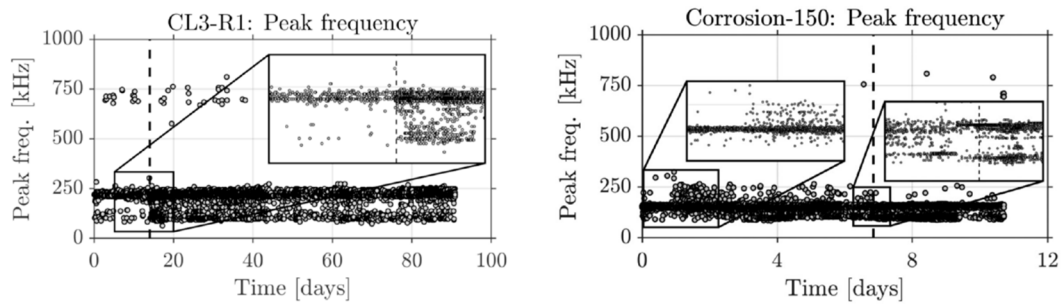


**Figure 8:** Peak frequency as a function of time during an accelerated corrosion test, (left) with flat response sensors (range 100-400 kHz), and (right) with 150 kHz resonance sensors, adapted from [60].

### 2.5.2 Moment tensor analysis

Alternative to the parameter-based analysis to distinguish between tensile and shear cracks as presented in section 2.4.3, a moment tensor analysis allows discriminating the crack type based on the entire waveform. Therefore, a simplified procedure, SiGMA (Simplified Green's functions for Moment tensor Analysis), was developed in which the source is localized in 3D and moment tensor analysis is performed [100]. The method allows estimating the size, orientation, location, and type of the crack. The signal should be recorded by at least six sensors in order to perform the analysis.

It was found that the onset of corrosion is characterized by shear and mixed-mode cracks [54]. Later on, more tensile cracks are formed around the rebar [54, 59, 68, 69]. Afterwards, mainly shear cracks are found as the cracks coalesce [59, 68, 69]. Ohno and Ohtsu [56] reported that the SiGMA analysis gave similar results as the RA-AF analysis during a hydrostatic expansion test mimicking the internal pressure due to corrosion products. Kawasaki et al. [69] discussed that the location of the surface crack was in agreement with the localized events that indicated mode II (shear crack), whereas the localized events indicating mode I (tensile crack) were distributed along the rebar.

Although reported results are consistent, the required data quality and quantity makes this technique cumbersome to apply for real-life corrosion monitoring on large-scale structures.

## 2.6 Clustering

Clustering and classification of AE signals is gaining more and more attention in the AE field, however, it has only been applied to a limited extent to signals obtained during the (accelerated) corrosion process. Clustering aims to group a data set into an amount of subsets or clusters, and is usually based on a distance measure that is representative of certain signal characteristics. It can find an internal structure in the data that was not known beforehand. Examples of clustering algorithms are k-means, fuzzy c-means, self-organizing map (SOM), and hierarchical clustering [101]. In classification, new data is assigned to predefined classes based on a training set. Examples are support vector machines (SVM) and neural networks [101].

Clustering and classification can be performed based on AE parameters or based on the entire waveform. Parameter-based clustering has mainly been discussed in the literature for characterization of damage in composites [102-104]. So far, parameter-based clustering or classification has not been performed during (accelerated) corrosion tests on reinforced concrete, as the values of parameters of different AE sources may be overlapping [60].

In addition, limited work has been performed on signal-based clustering during an accelerated corrosion process. The work of Calabrese et al. [82] has been mentioned before. In this research, a set of algorithms was combined to remove environmental noise during corrosion monitoring of a post-tensioned concrete beam. In this work, clustering was not performed to distinguish between sources originating from the corrosion process itself or concrete cracking. Van Steen et al. [50] developed a correlation-based agglomerative hierarchical clustering algorithm to distinguish groups of AE signals during the corrosion of small cylindrical mortar samples (diameter 36 mm). Signals from corrosion and concrete cracking were successfully distinguished. The results were validated by means of X-ray scans that allowed spatially distinguishing the AE sources in 3D visualizations of the internal cracks and corrosion products [50].

## **2.7 Overview of best-practice protocols for AE monitoring during corrosion tests**

The discussed protocols for AE data analysis for corrosion testing are summarized in Table 3 together with some specific requirements, characteristics, and remarks. The first column summarizes the AE analysis protocols. The second, third, and fourth column indicate three statements, respectively if the entire history is required to perform the analysis, if the analysis technique consistently leads to similar conclusions in the literature, and if the protocol can be applied for source identification. Whether the statement is valid, partially valid, or not valid is indicated by +, + / -, and - respectively. The fifth column shows important remarks concerning the applicability of the method.

In the second column concerning the required availability of the entire history, a negative mark (–) is preferred. If the entire history is needed for the data analysis method to be reliable, the specific method is less applicable for on-site monitoring in cases where the structure is already damaged. An example is the use of the cumulative rate for quantification of the damage level in which an increase is assigned to an increase in damage level. Yet, cumulative data might still be interesting to evaluate ongoing corrosion activity as a function of environmental parameters or external loads. For RA-AF analysis, this statement is partially valid. When RA and AF are plotted against each other, the entire history is not required, unless the limit to distinguish between mode I and mode II is based on maximum values obtained during testing.

In the third column, on the consistency of results within the literature, a positive mark (+) is preferred. This column is developed based on the information reported in the literature and presented in previous sections. Consistent results were found for most methods except for RA-AF analysis. For the intensity analysis ( $H(t)$ -Sr), consistent results were only found when these parameters are plotted as a function of time. When the parameters are plotted in comparison to specific limit values, several limits have been reported. Frequency analysis overall showed a decrease of the frequency over time, however, absolute

values seem to depend on the sensor type. As very limited research has been performed on clustering, this is indicated as + / - in this column. It should be noted that some inconsistency in results is expected, especially for those analysis methods where the results are influenced by specimen dimensions, test setup, AE sensor types and source-sensor distance. Hence, a proper mentioning of such aspects is highly important when AE studies are reported.

Also for the fourth column, representing the applicability of the method for source identification, a positive mark (+) is preferred. Source identification is of particular interest in case of corrosion as several AE sources are present and occurring at the same time in the same zone of the structure. This can lead to a more reliable assessment of the structure's condition and corrosion level, as it would allow to determine which damage process is ongoing. An RA-AF analysis and moment tensor analysis are able to identify tensile and shear cracks. Frequency analysis and clustering allow to identify AE sources such as corrosion and concrete cracking. A parameter-based analysis may be able to identify sources, however, the application during accelerated corrosion in RC is still limited and may not be reliable due to overlapping values. Source localization cannot directly identify sources, however, it can give additional information to validate results, e.g. sources around the rebar are more likely to originate from corrosion and sources closer to the surface are more likely to originate from concrete cracking.

**Table 3:** Summary of AE data analysis protocols including specific requirements, characteristics, and remarks, with + indicating that the statement above is valid, + / - indicating that it is partially valid, and – indicating that it is not valid.

analysis method	entire history needed?	consistent results in the literature?	applicable for source identification?	remarks
cumulative rate	+	+	-	Important to validate sudden increases with other AE methods or monitoring techniques
parameter analysis	-	+	+ / -	Specific parameter values are sample size and setup dependent
RA-AF analysis	+ / -	+ / -	+	Results may be affected by the applied sensor types and filters, and the source-sensor distance
(i)B-value analysis	+ / -	+	-	May be difficult to scale up to larger structures where zones might be in different stages of the corrosion process
intensity analysis (H(t)-Sr)	+	+ / -	-	Results may be dependent on the source-sensor distance
frequency analysis	-	+ / -	+	Absolute values for AE source characteristics should be approached very carefully
moment tensor analysis	-	+	+	The required data quality and quantity makes this technique cumbersome to apply on-site
source localization (1D-2D-3D)	-	+	+ / -	Source identification only possible if different sources are spatially separated
clustering	-	+ / -	+	Limited research has been performed

This overview indicates that no data analysis method is capable of solving all questions. The quality of the AE analysis can therefore be improved by:

- a decent filtering protocol to improve the quality of the data that is used for the analysis
- a combination of several analysis methods
- a verification of AE results with other monitoring and measurement techniques

### **3. AE for condition assessment of corroded RC element during load tests**

Several researchers have studied the AE signals originating from mechanical testing of corroded RC elements. These mechanical tests include pull-out tests, compression tests and bending tests, and are mostly performed in laboratory environments, after corroding the samples to a target corrosion level, mostly with an impressed current. Pull-out tests focus on loss of bond strength caused by corrosion while compression and bending tests focus on the remaining structural capacity.

#### **3.1 Pull-out tests**

The bond between the reinforcing steel and concrete offers resistance by chemical adhesion, mechanical interlock and friction between both materials. Pull-out failure is typically described by a three-stage process: (1) loss of chemical adhesion, (2) reduced mechanical interlock and (3) failure by splitting or pull-out [105]. Van Steen et al. [62] performed pull-out tests on corroded rebars, while monitoring the samples with AE. They found that the three stages of the pull-out process could be distinguished by the cumulative AE activity. They also found that for smooth or heavily corroded rebars, phase 2 is skipped and phase 1 immediately transitions to phase 3. The corroded samples released most AE activity during pull-out of the rebar (phase 3) and AE sources were located over the entire bonded length of the rebar.

Lei et al. [106] observed two peaks in the number of AE events during pull-out tests on corroded RC samples. These two peaks matched with the initial micro-cracking and crack propagation, after which splitting failure of the specimens occurred. Abouhussien et al. [107] found similar successive stages during pull-out. The initiation of micro-cracking, onset of macro-cracking in the concrete core and failure were detected by changes in the slope of the cumulative amount of hits. The cumulative signal strength (CSS), severity ( $S_r$ ) and historic index ( $H(t)$ ) confirmed the micro-cracking by change in the slope of CSS and  $S_r$  and peaks of  $H(t)$ , representing chemical adhesion loss and friction at the concrete-steel interface. A second change of slope (CSS and  $S_r$ ) and peak ( $H(t)$ ) was reported to be caused by the onset of macro-cracking in the concrete. Additionally, they observed that an increased bond length and larger concrete cover resulted in increased values of the AE parameters [107].

For samples with an increased corrosion level, a decrease in AE parameters was reported [106, 107]. During micro-cracking, this decrease can be explained by the weakened chemical adhesion and reduced confinement of the cracked concrete, which reduces the frictional resistance. Thereafter, macro-cracking is accompanied by a lower dowel contribution of the rebars' ribs that are partially corroded away and by signal attenuations due to cracks. Both effects cause a reduction of the AE parameters such as amplitude and energy during macro-cracking.

### 3.2 Compression tests

Researchers have recently studied the axial compression capacity of corroded RC columns while monitoring with AE [108, 109]. Li et al. [109] observed a more gradual release of AE energy for a corroded column in comparison to a non-corroded column. Already for low loading levels, energy was released by crack propagation because of the pre-existing cracks caused by corrosion. Therefore, also more AE hits are registered at low load levels for the corroded column, while the non-corroded column still deformed elastically and did not release much energy. Chen et al. [108] observed a similar trend for the cumulative AE hits. While the non-corroded column showed a steep increase in cumulative AE hits at the end of loading, the severely corroded columns already showed a steady increase at the beginning of the load test. This behavior seems to contradict the AE activity observed during bending or pull-out tests on corroded RC samples, where less AE activity was reported for increased corrosion levels. This might be due to the difference in fracture mechanisms during the different mechanical tests.

### 3.3 Bending tests

Most experimental research on AE monitoring of corroded RC structural components reported in the literature focusses on bending tests of corroded beams. Abouhussien et al. [110] studied bond strength during four-point bending tests. The tested beams were corroded along their anchorage length at one side, and monitored with AE. Similar to the pull-out tests reported in [107], flexural cracking, bond-slip and anchorage cracking was accompanied by a jump in  $H(t)$  and sudden increase of the slope of the cumulative AE hits, CSS and  $S_r$ . Although increasing the corrosion level did not modify these AE parameters during flexural cracking, on average the parameters did decrease during bond-slip and anchorage cracking.

The cumulative number of AE hits is a straightforward parameter to differentiate between different stages of the fracture process and therefore often applied during bending tests, which typically have a relatively short duration. Garhwal et al. [111] distinguished micro-cracking, a calm phase, macro-cracking and failure based on cumulative AE hits (Figure 9). Additionally, the number of AE hits was reduced for beams with a higher corrosion level. Moreover, the transitions between the phases diminished at very high corrosion levels ( $\geq 24.3\%$ ). Yoon et al. [99, 112] and Kawasaki et al. [113] also reported a decrease of the cumulative amount of AE hits with increasing corrosion level or  $Cl^-$  concentration, respectively. This effect of corrosion is explained by the formation of micro-cracks and longitudinal macro-cracks during the corrosion process before loading the beams, which already dissipates energy and increases AE signal attenuation. Additionally, the bond is deteriorated and the transfer of stresses to concrete is reduced. Shahid et al. [114] observed a similar decrease of the signal strength for corroded beams. However, the work of Gao et al. [115] contradicts the statement that the cumulative AE hits decrease with increasing corrosion level, as seen in Figure 10. Yet, the corrosion levels of the beams in their tests cover a limited range and are rather low. This might have caused only limited corrosion cracking and thus hinders a clear differentiation between cumulative AE results for the beam tests. In addition, whilst the other studies focused on flexural behavior, the beams tested by Gao et al. were designed as shear-critical beams, resulting in different failure modes. Hence, the results of these studies may not be directly comparable.

Next to the cumulative amount of hits, Yoon et al. [99, 112] also studied cross-plots. These show the relation of the amplitude of the signals to their duration. During the debonding and failure phases of the beams, the corroded samples produced AE events with shorter durations and higher amplitudes.

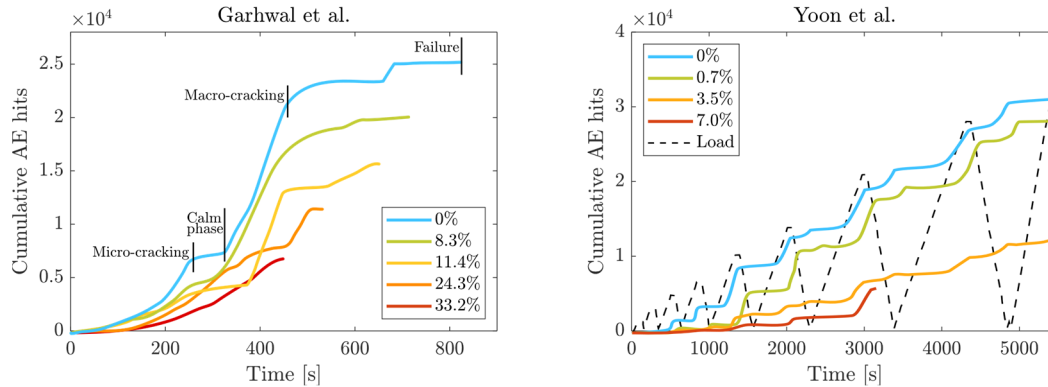


**Figure 9:** Cumulative amount of AE hits during monotonic [111] and cyclic [99] four-point bending tests of beams with different corrosion levels. On the left, four phases are indicated for the uncorroded beam. Average rebar mass loss is indicated in %. Data are originally reported in [111] and [99] and reproduced here in a similar format for ease of comparison.

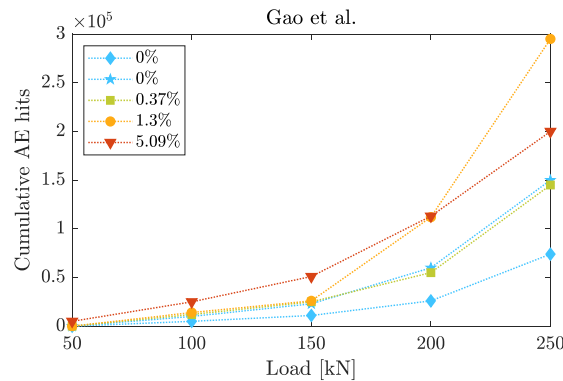


**Figure 10:** Cumulative amount of AE hits for five load steps during three-point bending of beams with different corrosion levels [115]. Average rebar mass loss is indicated in %. Data are adapted from [115] and reformatted for ease of comparison.

Zaki et al. [116] observed damage progress during three-point bending tests on corroded RC beams, by performing AF/RA analysis. They observed that during micro-cracking, RA decreased and AF increased, indicating the occurrence of tensile cracks. Towards the end of the test, the opposite was observed as the beams showed shear failure. The highest corrosion level was distinguished by a lower AE energy, decrease of RA and increase of AF. The lower AE energy corresponds with the findings in Figure 9, where the AE activity decreases with an increase in corrosion level. A decrease of RA and increase of AF is an indication of the formation of tensile cracks. Zhang et al. [117] and Gao et al. [115], who both performed similar three-point bending tests, confirmed these observations with additional AF/RA analyses for beams with higher corrosion levels. However, this trend was not found by Kawasaki et al. [113] who performed four-point bending tests on corroded specimens. They mainly observed that for corroded beams at early

loading stages, the RA increased and AF decreased in comparison with non-corroded beams, indicating shear cracking. Also in the general literature, a shift towards shear/delamination failure is typically reported for beams with higher corrosion levels [118, 119]. Discrepancies in AF/RA analysis results reported in the literature were also found during the corrosion process (see Section 2.4.3).

Localization of the AE events during bending tests has mostly been successful [111, 112, 115, 120] and resulting AE source locations resemble the observed cracks well, especially after data filtering. However, Schechinger and Vogel [121] noticed that macro-cracking could severely hinder the localization possibilities. Therefore, care should be taken when interpreting the results.

Specifically for cyclic loading tests, progressive damage parameters such as the Felicity, Calm and Relaxation ratio are used [34]. They are defined as follows:

$$\text{Felicity ratio} = \text{LOAD ratio} = \frac{\text{Load at Onset of AE activity in this cycle}}{\text{Maximum load at the previous cycle}}$$

$$\text{CALM ratio} = \frac{\text{amount of AE events during unloading part of a cycle}}{\text{amount of AE events during full cycle (loading and unloading)}}$$

$$\text{Relaxation ratio} = \frac{\text{Average AE energy during unloading part of a cycle}}{\text{Average AE energy during loading part of a cycle}}$$

The Felicity ratio is a value related to the Kaiser effect, which stipulates that the onset of AE activity occurs after the previous maximum load has been exceeded [19]. The Kaiser effect is therefore referred to as “the memory of the material” as only at higher loads new micro-cracks will be formed. Undamaged materials therefore have a Felicity ratio equal to or greater than 1. When the material has been substantially damaged, its micro-structure becomes unstable and AE activity occurs already at lower load levels, with a Felicity ratio dropping below 1.

Yoon et al. [99, 112] performed cyclic four-point bending tests on corroded RC beams while monitoring the AE activity. They used the Felicity ratio to differentiate between different corrosion levels and observed that the Felicity ratio decreased faster during the cyclic loading process for beams with higher corrosion levels, see Figure 11 (left). This observation was attributed to the occurrence of sliding friction or rubbing in the corroded beams. Shahid et al. [114] performed similar tests on larger beams, see Figure 11 (right). They corroded three beams over 15, 30 and 40 days with a current of 100  $\mu\text{A}/\text{cm}^2$ . An indication of the obtained corrosion levels can be found by applying Faraday’s Law, resulting in 1.19%, 2.37% and 3.54%. These corrosion levels are rather low, which causes a less distinctive contrast between the AE results of the different beams.

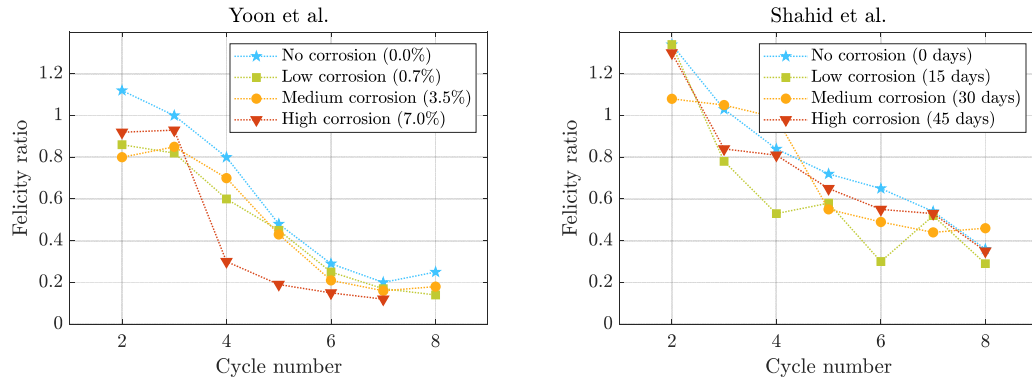


**Figure 11:** Evolution of the Felicity ratio for different corrosion degrees, from Yoon et al. [112] (left) and Shahid et al. [114] (right). Data are originally reported in [112] and [114] and reproduced here in a similar format for comparison.

While the Felicity or LOAD ratio focuses on reloading effects, the Relaxation and CALM ratio focus on AE activity during unloading. The Relaxation ratio is a measure for the amount of cracks present in the specimen. Cracks increase the amount of AE energy during unloading, resulting in higher relaxation ratios for more damaged beams. Although ElBatanouny et al. [120] could detect cracking of uncorroded beams by exceeding a Relaxation ratio of 1, no clear trends were observed for corroded, already cracked beams. On the other hand, Shahid et al. [114] did observe an increasing trend of the Relaxation ratio for corroded beams when the amount of cycles increased. When reaching around 40% of the ultimate load, the Relaxation ratio exceeded 1. Finally, Shahid et al. [114] also calculated the calm ratio during cyclic bending tests. This ratio increased as the amount of cycles or damage increased, for both corroded and uncorroded beams. The formation of new cracks or propagation of existing cracks was accompanied by a sudden increase in calm ratio.

In conclusion, although the investigated damage indicators were successfully used for quantifying cracking during cyclic loading, they did not always show clear correlations with the corrosion level of the RC beams.

#### 4. On-site AE monitoring of corroding RC structures

Up to this point, we focused on experimental testing in laboratory conditions, which simplifies the analysis of AE results as test conditions and environmental parameters can be controlled and tested RC components are relatively small. The transition to in-situ corrosion monitoring is challenging and scientific literature on this topic is limited. An overview on AE monitoring of RC structures was presented in [122]. This section gives an overview of reported on-site AE monitoring campaigns on corroded RC or PC structures. The detection and localization of wire breaks in PC structures, proof loading, and AE tomography will be discussed.

A successful on-site application of the AE technique in PC structures is the detection and localization of corrosion-induced failure of tendon wires, so-called wire breaks [123-126]. This type of failure is very sudden and characterized by high-energy elastic waves. In order to recognize and localize wire breaks, supporting laboratory tests [125], artificial wire breaks by an on-site accelerated corrosion setup [124], or

a corroding sample [125] may help to discriminate and identify AE signals from various sources. A dedicated study was performed by Yuyama et al. [125] in which small specimens were bonded to the structure. Noise due to traffic, hammering, and artificial wire breaks were detected and identified. It was found that wire breaks had the highest amplitudes. Preference was given to sensors with a resonance frequency of 55 kHz as too much traffic noise was recorded with a sensor having a lower resonance frequency (30 kHz) and signals were attenuated significantly for sensors with a higher resonance frequency (150 kHz). It was also reported in [125] that higher AE hit rates were observed during rush hours. Lower activity was observed during weekends and holidays. Similar AE event rate fluctuations were observed by Van Steen et al. [127] during an initial two-week monitoring campaign on corroded PC bridge girders. Additionally, differences between girders with varying corrosion crack widths and zones with high AE activity were observed and marked for further investigation [127]. Fricker and Vogel [124] were able to classify AE sources such as wire breaks, hammering, and concrete chipping. Blind tests were performed by attaching a galvanic corrosion cell at the bottom of the bridge to accelerate the corrosion process of a couple of wires with a direct current and sodium chloride solution. Therefore, spontaneous wire breaks could be classified during the monitoring period of 1 year.

Due to the specific working principles of the AE technique, only active damage can be detected, meaning that damage needs to occur when the structure is monitored. However for existing structures, it is also valuable to assess the already existing damage. Therefore, damage needs to be activated in order to be measurable with the AE technique. A currently applied technique to activate damage in PC or RC structures is proof loading using a static or moving load. For proof loading with a static load, the capacity of the structure is evaluated by applying a desired load condition, typically executed by applying increasing weights on a force frame [128]. For proof loading with a moving load, a heavy truck drives across a bridge in order to activate existing cracks. In both cases, deflections are monitored as well. By applying the AE technique during proof loading, several researchers were able to determine the damage level [33, 98, 129] and location of the damage [130] in existing concrete bridges. Nair and Cai [98] performed static and dynamic load tests during three consecutive days on a PC girder bridge. Amplitude-time plots show that AE signals were detected when the trucks passed. Observed amplitudes were low and not related to structural damage. An intensity analysis showed that no significant damage was developed during testing. Shiotani et al. [130, 131] expected severe damage in the middle of the span of a PC bridge after passage of a truck by investigating the CALM ratios and  $I_b$ -values. This was confirmed by lower velocities obtained with ultrasonic measurements. No damage was observed visually on the surface and therefore, a subsurface defect was assumed. Yang et al. [132] performed cyclic three-point bending tests on beams extracted from a 50 year old bridge, while monitoring them with AE. Several cracks were already observed in the specimens before loading. The CALM and LOAD ratio were obtained from the AE results, but the cumulative SS was used instead of the amount of AE events to calculate the CALM ratio. It was noticed that the CALM ratio was higher and the LOAD ratio was lower at the location where most flexural cracks were observed.

An extensive study in which three PC bridges and one RC bridge were monitored was presented by Golaski et al. [129]. Different analyses were performed. First, an intensity analysis on a newly built PC bridge confirmed that there was no damage. Second, static and dynamic loading of a severely damaged PC bridge

showed that in this case, static loading was more effective to detect existing damage. The bridge was again monitored after repair and the data did not indicate any active damage. Third, amplitudes of hits recorded in different zones were investigated under regular traffic for an old PC viaduct. Based on the amplitudes and AE activity, low, medium, and high intensity zones were identified. Fourth, AE monitoring was used to determine whether damage was induced during transportation of a heavy cargo load on an RC bridge. The measurements before, during, and after transportation did not suggest new damage. This elaborate study shows the potential of the AE technique for on-site monitoring, however, it was also reported that more research is needed to develop dedicated assessment protocols.

Alternatively, the application of tomography allows developing a wave velocity distribution profile. Lower velocities tend to point at higher damage levels [133]. As such, damaged zones can be localized. Two types of tomography exist, referred to as elastic wave tomography and AE tomography. For elastic wave tomography, sensors are attached on different sides of the structure. Ultrasonic pulses are passed from a series of transmitting sensors to receiving sensors at various locations around the structure. Usually, sensors are used as both transmitting and receiving sensor. Based on the arrival time of the pulses, the velocity profile is determined. For AE tomography, an external source such as a moving heavy truck is applied to activate the existing cracks (called secondary AE). Sensors are usually placed on one side of the structure [130, 131]. Shiotani et al. [131] performed pencil lead breaks to establish a velocity plot. Zones of lower velocity were observed, however, no visual damage could be seen and therefore a subsurface defect was expected. Recently, heavy rain was successfully used as an external source to localize delamination in an RC bridge deck using AE tomography [134]. Less AE events were localized in deteriorated zones with delamination, which was confirmed by core drilling. Despite the potential of AE tomography, no dedicated on-site measurements were reported in the literature for corrosion damage detection in existing RC structures.

## **5. Discussion and future challenges**

### **5.1 Overview and applicability of AE techniques**

Table 4 presents an overview of AE data availability in the literature. The availability of reported AE data for corrosion monitoring and testing of corroded RC samples and structures is indicated with colors from dark to pale grey, with higher availabilities of data indicated in darker greyscale values. If an analysis method is not applicable for a certain test type, this is mentioned as non-applicable (N.A.). The aim of this overview is to indicate gaps in the availability of data sets. Such gaps (light grey and white cells) point at either a research challenge still to be addressed, or at limited applicability or reliability of a certain AE method for a test type. It can be seen that most research challenges still to be addressed are situated in the columns related to on-site AE monitoring of corroding RC structures. Also the use of AE tomography for detection of corrosion damage, and a further extension of data sets on dedicated signal (frequency) analysis would be interesting research tracks. Specific challenges related to on-site corrosion monitoring are discussed in the next section.

**Table 4:** Overview of data availability in the literature, as a relation between AE data analysis protocols and test type. High availabilities indicated with darker greyscale values. If an analysis method is not applicable for a certain test type, this is indicated with N.A.

AE analysis method	Availability of data reported in the scientific literature			
	for (accelerated) corrosion testing	for mechanical testing in the lab	for on-site corrosion monitoring	for on-site test loading on corroded structures
cumulative rate				
parameter analysis				
RA-AF analysis				
iB-value analysis				
intensity analysis				
frequency analysis				
moment tensor analysis				
source localization (1D-2D-3D)				
clustering				
LOAD-CALM ratios	N.A.		N.A.	
AE tomography				

## 5.2 Further research challenges

Challenges related to specific AE methods were discussed throughout the paper, and research gaps related to availability of experimental data sets were illustrated in Table 4. It was observed that most challenges are focused towards on-site monitoring. Therefore, several specific challenges for further research are highlighted and discussed here.

### Robustness, flexibility and durability of on-site AE monitoring systems:

Sensors generally have a shorter lifetime than the structure on which they are installed. Additionally, it was shown that sensor-based techniques are typically tailored towards monitoring of a specific damage effect during (part of) the corrosion process in RC structures (see Table 1). As mentioned before, a combination of several techniques into a sensor network is considered to be the most robust approach [24]. Such approach enables to correlate a multitude of information regarding not only the corrosion process and damage effects, but also the environmental parameters. It also allows tailoring a network of sensors for covering (the relevant parts of) the whole corrosion process, adding and changing certain sensors to allow flexibility when damage effects increase. For example, higher-frequency AE sensors may capture the local corrosion damage initiation, while lower-frequency AE sensors can be tailored towards capturing the macro-cracking in concrete.

To enhance the durability of AE sensors, research has focused on embedding these sensors in the concrete in the form of smart aggregates [135-137]. Although this approach has advantages concerning the durability of the embedded sensors, their effect on the mechanical behavior of the host material and their reduced sensitivity are still under investigation. Further enhancements in sensor technology, such as wireless systems and energy harvesting, are expected to also boost the versatility and applicability of the AE technique for on-site monitoring of RC structures.

#### Data analysis and noise filtering:

It was shown in Figure 5 how the use of appropriate onset time picking and filtering algorithms may drastically improve the AE source localization, especially for 3D sensor setups. In addition, it is also clear from the literature analysis that the interpretation and classification of AE signals is not always straightforward, especially with regard to the corrosion process where many AE sources are active and not always spatially distinguishable.

During on-site monitoring, additional noise sources such as traffic noise can be expected, especially if lower-frequency AE sensors are applied. Increased AE activity was reported in the literature during periods with voluminous traffic loads [125, 127], although it has not yet been established whether the increased AE activity is due to environmental noise sources, increased damage rates, secondary AE such as friction in existing cracks or a combination of these.

To avoid noise or unwanted AE signals, a two-step approach is typically used in lab testing as well as on-site monitoring. Firstly, a proper choice of AE sensor sensitivity and band pass filters reduces the capturing of noise signals and secondly, the application of subsequent filtering techniques during data processing further reduces the amount of unwanted AE signals [19]. Filtering techniques were discussed before in this paper, and it was shown that signal-based filtering during post-processing is often required to distinguish between AE sources. As this requires an acquisition of the whole AE signal, storage of the transient waveforms and a pre-trigger part of the transient signal is required. Therefore, appropriate methods for big data analysis, such as automated clustering and (un-)supervised machine learning are needed in addition to careful benchmarking and dummy sensors, to enhance processing of AE data from noisy environments.

#### Real-time monitoring of slow degradation processes:

As the AE technique aims at capturing active, ongoing damage processes, the damage needs to occur while the structure is monitored. However for existing structures, it is valuable to be able to assess the location and severity of corrosion from a monitoring period that covers only a smaller part of the structure's lifetime. An additional difficulty here is the fact that corrosion is a very slow process that is influenced by environmental conditions such as temperature and moisture, hence it is not always active. Therefore, it may be needed to activate the ongoing damage process in order to be measurable with the AE technique.

Currently applied techniques to activate or visualize damage in RC structures such as proof loading and AE tomography were discussed in section 4. These techniques are mainly applied to activate existing cracks and produce secondary AE activity from fretting between crack surfaces, or to visualize the existing cracks by means of wave velocity profiles. The corrosion process itself and micro-cracking of concrete due to corrosion are characterized by low energy events, making them more challenging to study. Therefore, additional activation protocols to capture natural (slow) degradation processes in RC structures need further investigation. Moreover, also several other structures such as RC wall panels, walls, columns, and tunnels can show deterioration due to corrosion. For these applications, no damage activation method exists yet. Therefore, new damage activation protocols are needed to assess the already existing damage and the slow degradation progress in these types of structures.

#### From AE monitoring towards structural assessment:

In-situ inspection and monitoring may either focus on local damage detection and mechanical response characterization, or global structural performance evaluation. This implies that condition survey approaches are multi-scale, providing data with various spatial densities: point, grid, zonal and overall information. Point measurements are typically randomly distributed within the structure and/or located at zones of interest from visual inspection. Examples are core compressive strength, chloride content, local strain, etc. Grid measurements are taken at specific intervals along a line, e.g. a longitudinal crack, or at the nodes of a grid with a specific mesh size. In the latter case, data are typically extrapolated to heat plots (see figure 12). Examples of 1D and 2D grid measurements are crack width, potential mapping, cover thickness, ultrasonic velocity, etc. AE monitoring data can be taken as 1D grid data, e.g. the location of wire breaks in pre-stressing strands, or considered as zonal information. An example of the latter is a localization plot of AE sources that is presented as a heat plot. Aim of zonal localization of damage hotspots is often to indicate specific point locations for further inspection. And finally, the overall or global techniques give information about the global structural response. Examples are vibration velocities, frequency response spectrum, etc.

A major challenge in corrosion damage assessment in existing structures is therefore the coupling of data with various spatial and time scales. This coupling can be done through direct or weighted correlation between local and global damage observations (at specific points in time), or by means of model-based correlations in which spatial variability can be included via zonal gradient approaches.

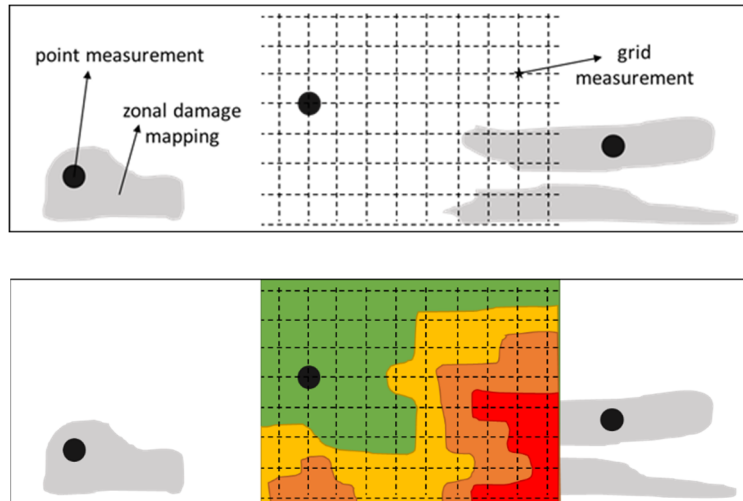


**Figure 12:** Inspection and monitoring data from point, grid and zonal locations (top), heat map of grid measurements and overlay with damage zones (bottom).

The strength of the AE technique lies in obtaining information of the damage process on a local scale, be it either as point, grid or zonal data. Coupling AE data to the global behavior of a structure remains challenging. However, up-scaling the acquired information could be beneficial to obtain knowledge about the structural performance of an existing, corroded structure and consequently determine the urgency of an intervention. Therefore, the development of a multi-scale monitoring approach is required. For instance, the combination of the local AE technique with the global vibration-based monitoring method could allow for a more accurate quantification of the structural capacity of deteriorated RC structures since both techniques can compensate for the shortcomings of the other. An example of such coupling by means of direct correlation between damage observations from local AE data and global modal frequencies was presented for mechanical bending tests in [138]. The coupling of local AE monitoring with global monitoring techniques, and the related reduction of uncertainties is to be elaborated in further research.

## 6. Conclusions

This paper presented an in-depth literature review and discussion on the AE technique for corrosion monitoring in RC. It was shown that AE monitoring has several important features that makes it have a vantage point over other techniques for RC corrosion monitoring, yet many challenges still need to be addressed and an ill-informed use of the technique might lead to erroneous results. In addition, no specific standards for AE-based corrosion monitoring in RC structures currently exist.

Firstly, AE-based damage monitoring during accelerated corrosion tests is discussed, including AE setups, methods for filtering and data analysis, and best-practice protocols as deduced from the literature study. An overview is presented of methods for parameter- and signal-based analysis, with indication of consistency of results reported in the literature. It is found that many AE methods provide consistent results (cumulative rate, parameter analysis, moment-tensor analysis, (i)b-value analysis), yet they may

be difficult to upscale to on-site monitoring as the whole history is needed, or required data quality and quantity puts high requirements on AE acquisition systems.

Secondly, application of the AE technique for condition assessment of corroded RC elements during load testing is discussed. The literature overview focused on pull-out, compression and bending tests, with most research results being reported on the latter. It is found that less AE hits and lower felicity ratios are reported in the literature for beams with higher corrosion levels, yet also some inconsistent results were found. It is concluded that the investigated damage indicators proved very useful in capturing damage progress during testing, however, AE results did not always show clear correlations with the corrosion level of the RC beams.

Hereafter, an overview is presented of on-site AE monitoring campaigns on corroding RC structures reported in the literature. A discussion on the availability of data for corrosion monitoring in lab and in-situ, as well as for test loading on corroded structural components in lab and in-situ showed that most research challenges are related to in-situ monitoring of corrosion damage in RC structures. Following aspects were highlighted:

- Robustness, flexibility and durability of on-site AE monitoring systems requires further development of sensor networks, embedded sensors, wireless systems and energy harvesting techniques.
- For RC corrosion monitoring in noisy environments, storage of the AE transient waveforms is needed for enhanced data analysis and noise filtering by means of big data analysis protocols.
- Real-time AE monitoring of slow degradation processes such as RC corrosion requires the development of dedicated damage activation protocols.
- To progress from AE monitoring towards structural assessment, research should focus on coupling of data with various spatial and time scales, and the development of multi-scale monitoring approaches.

### Acknowledgements

The financial support from FWO-Flanders (grant numbers 12ZD221N and SB/1SC1921N) and KU Leuven Internal Funds (project C24/17/042) is gratefully acknowledged.

### References

1. Brueckner, R. and P. Lambert, *Unexpected effects of historic concrete innovations*. Journal of Heritage Architecture, 2017. **1**(4): p. 549-563.
2. Fédération internationale du béton (fib), *Condition control and assessment of reinforced concrete structures exposed to corrosive environments (carbonation/chlorides)*, fib bulletin 59. 2011.
3. *Highways and Bridges [last accessed 4 May 2021]*. Available from: <https://www.nace.org/resources/industries-nace-serves/highways-bridges>.
4. Malomo, D., et al., *Numerical Study on the Collapse of the Morandi Bridge*. ASCE Journal of Performance of Constructed Facilities, 2020. **34**(4): p. 04020044.
5. Elsener, B., *Macrocell corrosion of steel in concrete - implications for corrosion monitoring*. Cement and Concrete Composites, 2002. **24**(1): p. 65-72.

6. Liu, J., et al., *Understanding the interacted mechanism between carbonation and chloride aerosol attack in ordinary Portland cement concrete*. Cement and Concrete Research, 2017. **95**: p. 217-225.
7. Broomfield, J.P., *Corrosion of Steel in Concrete: understanding, investigation and repair*. 2007: Taylor & Francis.
8. Fédération internationale du béton (fib), *Bulletin 34: Model Code for Service Life Design*. 2006. 116.
9. Tuutti, K., *Corrosion of steel in concrete*. 1982, Stockholm, Sweden: Swedish Cement and Concrete Research Institute.
10. Cigna, R., U. Nürnberger, and C. Andrade, *COST Action 521: Corrosion of steel in reinforced structures: final report*. 2003.
11. Raczkiwicz, W. and A. Wojcicki, *Temperature Impact on the Assessment of Reinforcement Corrosion Risk in Concrete by Galvanostatic Pulse Method*. Applied Sciences, 2020. **10**(3): p. 1089.
12. Luo, D., et al., *A Recent Progress of Steel Bar Corrosion Diagnostic Techniques in RC Structures*. Sensors, 2018. **19**(34): p. 1-30.
13. CONTECVET, *A validated users manual for assessing the residual life of concrete structures - Manual for assessing corrosion-affected concrete structures (downloaded from [www.ietcc.csic.es](http://www.ietcc.csic.es), September 2019), EC Innovation Programme, IN309021*. 2001.
14. Raupach, M. and P. Schießl, *Macrocell sensor systems for monitoring of the corrosion risk of the reinforcement in concrete structures*. NDT & E International, 2001. **34**(6): p. 435-442.
15. Tang, F., et al., *A review on fiber optic sensors for rebar corrosion monitoring in RC structures*. Construction and Building Materials, 2021. **313**: p. 125578.
16. Yeih, W. and R. Huang, *Detection of the corrosion damage in reinforced concrete members by ultrasonic testing*. Cement and Concrete Research, 1998. **28**(7): p. 1071-1083.
17. Watanabe, T., et al., *Evaluation of corrosion-induced crack and rebar corrosion by ultrasonic testing*. Construction and Building Materials, 2014. **67**: p. 197-201.
18. Sharma, A., et al., *Investigation of deterioration in corroding reinforced concrete beams using active and passive techniques*. Construction and Building Materials, 2018. **161**: p. 555-569.
19. Grosse, C.U., et al., eds. *Acoustic Emission Testing - Basics for Research - Applications in Engineering*. 2021, Springer.
20. Zaki, A., et al., *Non-Destructive Evaluation for Corrosion Monitoring in Concrete: A Review and Capability of Acoustic Emission Technique*. Sensors, 2015. **15**(8): p. 19069-19101.
21. Hassan, M.I. and N. Yazdani, *An Experimental Study for Quantitative Estimation of Rebar Corrosion in Concrete Using Ground Penetrating Radar*. Journal of Engineering, 2016. **2016**: p. 1-9.
22. Hong, S., et al., *Long-term monitoring of reinforcement corrosion in concrete using ground penetrating radar*. Corrosion Science, 2017. **114**: p. 123-132.
23. Fédération internationale du béton (fib), *Bulletin 59: Condition control and assessment of reinforced concrete structures exposed to corrosive environments (carbonation/chlorides)*. 2011.
24. The international Federation of Structural Concrete (fib), *Monitoring and safety evaluation of existing concrete structures. State-of-art report. fib bulletin 22*. 2003.
25. Li, Z., et al., *Corrosion mechanism of reinforced bars inside concrete and relevant monitoring or detection apparatus: A review*. Construction and Building Materials, 2021. **279**: p. 122432.
26. Montemor, M.F., A.M.P. Simões, and M.G.S. Ferreira, *Chloride-induced corrosion on reinforcing steel: from the fundamentals to the monitoring techniques*. Cement and Concrete Composites, 2003. **25**: p. 491-502.

27. Fan, L. and X. Shi, *Techniques of corrosion monitoring of steel rebar in reinforced concrete structures: A review*. Structural Health Monitoring, 2021: p. 14759217211030911.
28. CEN, *EN 1330-9: Non-destructive testing - Terminology - Part 9: Terms used in acoustic emission testing*. 2017.
29. Verstrynge, E., et al., *A review on acoustic emission monitoring for damage detection in masonry structures*. Construction and Building Materials, 2020: p. 121089.
30. Van Steen, C. and E. Verstrynge, *Degradation Monitoring in Reinforced Concrete with 3D Localization of Rebar Corrosion and Related Concrete Cracking*. Applied Sciences, 2021. **11**(15): p. 6772.
31. ASTM International, *ASTM E569 / E569M-13, Standard Practice for Acoustic Emission Monitoring of Structures During Controlled Stimulation*. 2013: West Conshohocken, PA.
32. De Santis, S. and A.K. Tomor, *Laboratory and field studies on the use of acoustic emission for masonry bridges*. Ndt & E International, 2013. **55**: p. 64-74.
33. Yang, Y., D.A. Hordijk, and A. de Boer, *Acoustic emission measurement in the proof loading of an existing bridge affected by ASR*, in *5th International Symposium on Life-Cycle Civil Engineering: IALCCE 2016, Life-Cycle of Engineering Systems: Emphasis on Sustainable Civil Infrastructure*, J. Bakker, D.M. Frangopol, and K. van Breugel, Editors. 2016, Taylor & Francis Group: Delft, The Netherlands.
34. *ISO 16837:2019: Non-destructive testing — Acoustic emission testing — Test method for damage qualification of reinforced concrete beams*
35. Carpinteri, A., S. Invernizzi, and G. Lacidogna, *Structural Assessment of a 17th-Century Masonry Vault with Acoustic Emissions and Numerical Techniques*. International Journal of Architectural Heritage, 2007. **1**(2): p. 214–226.
36. CEN, *EN 13477-1:2001 - Non-destructive testing - Acoustic emission - Equipment characterisation - Part 1: Equipment description*. 2001.
37. CEN, *EN 13477-2: 2021 Non-destructive testing - Acoustic emission testing - Equipment characterisation - Part 2: Verification of operating characteristics*. 2021.
38. CEN, *EN 13554:2011 Non-destructive testing - Acoustic emission testing - General principles*. 2011.
39. *ISO 12716:2001 Non-destructive testing — Acoustic emission inspection — Vocabulary*. 2001.
40. *ISO 12713:1998 Non-destructive testing — Acoustic emission inspection — Primary calibration of transducers*. 1998.
41. *ISO 16836:2019: Non-destructive testing — Acoustic emission testing — Measurement method for acoustic emission signals in concrete*.
42. *ISO 16838:2019: Non-destructive testing — Acoustic emission testing — Test method for classification of active cracks in concrete structures*.
43. Ohtsu, M., *Recommendation of RILEM TC 212-ACD: acoustic emission and related NDE techniques for crack detection and damage evaluation in concrete*. Materials and Structures, 2010. **43**(9): p. 1183-1186.
44. Ohtsu, M., ed. *Innovative AE and NDT techniques for On-Site Measurement of Concrete and Masonry Structures: State-of-the-Art Report of the RILEM Technical Committee 239-MCM*. RILEM State-of-the-Art Reports. Vol. 20. 2016, Springer Netherlands.
45. JSNDI, *NDIS 2421 Recommended practice for in-situ monitoring of concrete structures by acoustic emission*. 2000: Tokyo.
46. Patil, S., B. Karkare, and S. Goyal, *Acoustic emission vis-a-vis electrochemical techniques for corrosion monitoring of reinforced concrete element*. Construction and Building Materials, 2014. **68**: p. 326-332.

47. Patil, S., S. Goyal, and B. Karkare, *Acoustic emission-based mathematical procedure for quantification of rebar corrosion in reinforced concrete*. Current Science, 2015. **109**(5): p. 943-948.
48. Li, W., et al., *Monitoring Concrete Deterioration Due to Reinforcement Corrosion by Integrating Acoustic Emission and FBG Strain Measurements*. Sensors, 2017. **17**(657): p. 1-12.
49. Idrissi, H. and A. Limam, *Study and characterization by acoustic emission and electrochemical measurements of concrete deterioration caused by reinforcement steel corrosion*. NDT and E International, 2003. **36**: p. 563-569.
50. Van Steen, C., et al., *Localisation and characterisation of corrosion damage in reinforced concrete by means of acoustic emission and X-ray computed tomography*. Construction and Building Materials, 2019. **197**: p. 21-29.
51. Assouli, B., et al., *Detection and identification of concrete cracking during corrosion of reinforced concrete by acoustic emission coupled to the electrochemical techniques*. NDT and E International, 2005. **38**: p. 682-689.
52. Yu, A.-P., et al., *An experimental study of corrosion damage distribution of steel bars in reinforced concrete using acoustic emission technique*. Construction & building materials, 2020. **254**: p. 119256.
53. Di Benedetti, M., et al., *Acoustic emission historic index and frequency spectrum of reinforced concrete under accelerated corrosion*. Journal of Materials in Civil Engineering, 2014. **26**(9): p. 1-8.
54. Kawasaki, Y., et al., *Corrosion mechanisms in reinforced concrete by acoustic emission*. Construction and Building Materials, 2013. **48**: p. 1240-1247.
55. Di Benedetti, M., et al., *Acoustic Emission Monitoring of Reinforced Concrete under Accelerated Corrosion*. Journal of Materials in Civil Engineering, 2013. **25**: p. 1022-1029.
56. Ohno, K. and M. Ohtsu, *Crack classification in concrete based on acoustic emission*. Construction and Building Materials, 2010. **24**(12): p. 2339-2346.
57. Uddin, F.A.K.M. and M. Ohtsu, *Micromechanics of corrosion cracking in concrete by AE-SIGMA*. Journal of Acoustic Emission, 2005. **23**: p. 136-142.
58. Abouhussien, A.A. and A.A.A. Hassan, *The Use of Acoustic Emission Intensity Analysis for the Assessment of Cover Crack Growth in Corroded Concrete Structures*. Journal of Nondestructive Evaluation, 2016. **35**(52): p. 1-14.
59. Kawasaki, Y., Y. Tomoda, and M. Ohtsu, *AE monitoring of corrosion process in cyclic wet-dry test*. Construction and Building Materials, 2010. **24**: p. 2353-2357.
60. Van Steen, C., et al., *Acoustic emission source characterisation of chloride-induced corrosion damage in reinforced concrete*. Structural Health Monitoring, 2021. **Advanced online publication**: p. 1-21.
61. Elfergani, H.A., R. Pullin, and K.M. Holford, *Damage assessment of corrosion in prestressed concrete by acoustic emission*. Construction and Building Materials, 2013. **40**: p. 925-933.
62. Van Steen, C., et al., *Assessing the bond behaviour of corroded smooth and ribbed rebars with acoustic emission monitoring*. Cement and Concrete Research, 2019. **120**: p. 176-186.
63. Mangual, J., et al., *Acoustic-emission-based characterization of corrosion damage in cracked concrete with prestressing strand*. ACI Materials Journal, 2013. **110**(1): p. 89-98.
64. Dubuc, B., A. Ebrahimkhanlou, and S. Salamone, *Corrosion monitoring of prestressed concrete structures by using topological analysis of acoustic emission data*. Smart Materials and Structures, 2019. **28**: p. 055001.
65. Li, Z., et al., *Application of Acoustic Emission Technique to Detection of Reinforcing Steel Corrosion in Concrete*. ACI Materials Journal, 1998. **95**: p. 68-76.

66. Ing, M., S. Austin, and R. Lyons, *Cover zone properties influencing acoustic emission due to corrosion*. Cement and Concrete Research, 2005. **35**: p. 284-295.
67. Abouhussien, A.A. and A.A.A. Hassan, *Evaluation of damage progression in concrete structures due to reinforcing steel corrosion using acoustic emission monitoring*. Journal of Civil Structural Health Monitoring, 2015. **5**(5): p. 751-765.
68. Ohtsu, M., K. Mori, and Y. Kawasaki, *Corrosion process and mechanisms of corrosion-induced cracks in reinforced concrete identified by AE analysis*. Strain, 2011. **47**(2): p. 179-186.
69. Kawasaki, Y., T. Kobara, and M. Ohtsu, *Kinematics of Corrosion Damage Monitored by Acoustic Emission Techniques and Based on a Phenomenological Model*. Journal of Advanced Concrete Technology, 2012. **10**: p. 160-169.
70. Sharma, A., et al., *Monitoring invisible corrosion in concrete using a combination of wave propagation techniques*. Cement & concrete composites, 2018. **90**: p. 89-99.
71. Li, Z., et al., *Combined application of novel electromagnetic sensors and acoustic emission apparatus to monitor corrosion process of reinforced bars in concrete*. Construction & building materials, 2020. **245**: p. 118472.
72. ElBatanouny, M.K., et al., *Early corrosion detection in prestressed concrete girders using acoustic emission*. Journal of Materials in Civil Engineering, 2014. **26**(3): p. 504-511.
73. Abouhussien, A.A. and A.A.A. Hassan, *Acoustic emission monitoring of corrosion damage propagation in large-scale reinforced concrete beams*. Journal of Performance of Constructed Facilities, 2018. **32**(2): p. 04017133.
74. Appalla, A., et al., *Assessing Corrosion Damage in Posttensioned Concrete Structures Using Acoustic Emission*. Journal of Materials in Civil Engineering, 2016. **28**(2): p. 0415128.
75. Mangual, J., et al., *Corrosion Damage Quantification of Prestressing Strands Using Acoustic Emission*. Journal of Materials in Civil Engineering, 2013. **25**(9): p. 1326-1334.
76. Ohtsu, M. and Y. Tomoda, *Phenomenological Model of Corrosion Process in Reinforced Concrete Identified by Acoustic Emission*. ACI Materials Journal, 2008. **105**(2): p. 194-199.
77. Leelalerkiet, V., et al., *Estimation of Corrosion in Reinforced Concrete by Electrochemical Techniques and Acoustic Emission*. Journal of Advanced Concrete Technology, 2005. **3**(1): p. 137-147.
78. Ohtsu, M. and Y. Tomoda, *Corrosion Process in Reinforced Concrete Identified by Acoustic Emission*. Materials Transactions, 2007. **48**(6): p. 1184-1189.
79. Zheng, Y., et al., *Localized corrosion induced damage monitoring of large-scale RC piles using acoustic emission technique in the marine environment*. Construction and Building Materials, 2020. **243**: p. 118270.
80. Velez, W., F. Matta, and P. Ziehl, *Acoustic emission monitoring of early corrosion in prestressed concrete piles*. Structural Control and Health Monitoring, 2015. **22**: p. 873-887.
81. Zheng, Z., X. Sun, and Y. Lei, *Monitoring corrosion of reinforcement in concrete structures via fiber Bragg grating sensors*. Frontiers of Mechanical Engineering in China, 2009. **4**(3): p. 316-319.
82. Calabrese, L., G. Campanella, and E. Proverbio, *Noise removal by cluster analysis after long time AE corrosion monitoring of steel reinforcement in concrete*. Construction and Building Materials, 2012. **34**: p. 362-371.
83. Zhang, F., L. Pahlavan, and Y. Yang, *Evaluation of acoustic emission source localization accuracy in concrete structures*. Structural Health Monitoring, 2020. **16**(6): p. 2063-2074.
84. Gollob, S., et al., *A novel multi-segment path analysis based on a heterogeneous velocity model for the localization of acoustic emission sources in complex propagation media*. Ultrasonics, 2017. **74**: p. 48-61.

85. Ge, M., *Analysis of source location algorithms Part I: Overview and non-iterative methods*. Journal of Acoustic Emission, 2003. **21**: p. 14-24.
86. Ge, M., *Analysis of Source Location Algorithms, Part II: Iterative Methods*. Journal of Acoustic Emission, 2003. **21**: p. 29-51.
87. Geiger, L., *Probability method for the determination of earthquake epicenters from the arrival time only*. Bulletin of Saint Louis University, 1912. **8**(1): p. 56-71.
88. Gollob, S., *Source localization of acoustic emissions using multi-segment paths based on a heterogeneous velocity model in structural concrete*. 2017, ETH Zurich.
89. Yu, A.-P., et al., *An experimental study of corrosion damage distribution of steel bars in reinforced concrete using acoustic emission technique*. Construction and Building Materials, 2020. **254**: p. 119256.
90. Vandecruys, E., et al., *Acoustic emission sensing an vibration-based monitoring of corroded reinforced concrete beams*, in *The International Symposium on Nondestructive Testing in Civil Engineering (NDT-CE)*. 2022: Zurich, Switzerland.(in preparation)
91. Vandecruys, E., et al., *Acoustic emission monitoring of the chloride-induced corrosion process in reinforced concrete*, in *First Conference of the European Association on Quality Control of Bridges and Structures (Eurostruct 2021)*. 2021: Padova, Italy.
92. Vidya Sagar, R. and P. Raghu, B. K., *A review of recent developments in parametric based acoustic emission techniques applied to concrete structures*. Nondestructive Testing and Evaluation, 2012. **27**(1): p. 47-68.
93. Aggelis, D.G., et al., *The influence of propagation path on elastic waves as measured by acoustic emission parameters*. Structural Health Monitoring, 2012. **11**(3): p. 359-366.
94. Livitsanos, G., et al., *Numerical simulation of elastic wave propagation in masonry compared with acoustic emission experimental results*. Archives of Civil and Mechanical Engineering, 2020. **20**(1): p. 1-11.
95. Colombo, S., I.G. Main, and M.C. Forde, *Assessing Damage of Reinforced Concrete Beam Using "b-value" Analysis of Acoustic Emission Signals*. Journal of Materials in Civil Engineering, 2003. **15**(3): p. 280-286.
96. Carpinteri, A., G. Lacidogna, and S. Puzzi, *From criticality to final collapse: Evolution of the "b-value" from 1.5 to 1.0*. Chaos Solitons & Fractals, 2009. **41**(2): p. 843-853.
97. Shiotani, T., et al., *Evaluation of progressive failure using AE sources and improved b-value on slope model tests*. Progress in Acoustic Emission VII, 1994. **7**: p. 529-534.
98. Nair, A. and C.S. Cai, *Acoustic emission monitoring of bridges: Review and case studies*. Engineering Structures, 2010. **32**: p. 1704-1714.
99. Yoon, D.-J., W.J. Weiss, and S.P. Shah, *Assessing Damage in Corroded Reinforced Concrete Using Acoustic Emission*. Journal of engineering mechanics, 2000. **126**(3): p. 273-283.
100. Ohtsu, M., T. Okamoto, and S. Yuyama, *Moment Tensor Analysis of Acoustic Emission for Cracking Mechanisms in Concrete*. ACI Structural Journal, 1998. **95**(2): p. 87-95.
101. Maimon, O. and L. Rokach, *Data mining and knowledge discovery handbook*. 2005: Springer.
102. Li, L., et al., *Cluster analysis of acoustic emission signals for 2D and 3D woven glass-epoxy composites*. Composite Structures, 2014. **116**: p. 286-299.
103. Saeedifar, M., et al., *Clustering of interlaminar and intralaminar damages in laminated composites under indentation loading using Acoustic Emission*. Composites Part B, 2018. **144**: p. 206-219.
104. Zhou, W., et al., *Cluster analysis of acoustic emission signals and deformation measurement for delaminated glass fiber epoxy composites*. Composite Structures, 2018. **195**: p. 349-358.
105. Fédération internationale du béton (fib), *Bulletin 10: Bond of Reinforcement in Concrete*. 2000.

106. Lei, W., et al., *Experimental study of a pull-out test of corroded steel and concrete using the acoustic emission monitoring method*. Construction & building materials, 2016. **122**: p. 163-170.
107. Abouhussien, A.A. and A.A.A. Hassan, *Acoustic emission-based analysis of bond behavior of corroded reinforcement in existing concrete structures*. Structural Control and Health Monitoring, 2017. **24**: p. 1-18.
108. Chen, Y., et al., *Acoustic Emission Study on the Damage Evolution of a Corroded Reinforced Concrete Column under Axial Loads*. Crystals (Basel), 2021. **11**(1): p. 67.
109. Li, Q., et al., *Acoustic Emission Analysis of Corroded Reinforced Concrete Columns under Compressive Loading*. Sensors (Basel, Switzerland), 2020. **20**(8): p. 2412.
110. Abouhussien, A.A. and A.A.A. Hassan, *Application of acoustic emission monitoring for assessment of bond performance of corroded reinforced concrete beams*. Structural health monitoring, 2017. **16**(6): p. 732-744.
111. Garhwal, S., S. Sharma, and S.K. Sharma, *Acoustic Emission Monitoring of RC Beams Corroded to Different Levels Under Flexural Loading*. Arabian journal for science and engineering (2011), 2021. **46**(5): p. 4319-4335.
112. Yoon, D.-J., W.J. Weiss, and S.P. Shah, *Detecting the extent of corrosion with acoustic emission*. Transportation research record, 2000. **1698**(1698): p. 54-60.
113. Kawasaki, Y., et al., *Evaluation for RC specimen damaged from rebar corrosion by acoustic emission technique*. Construction & building materials, 2014. **67**: p. 157-164.
114. Shahid, K.A., et al., *Assessment of corroded reinforced concrete beams: Cyclic load test and acoustic emission techniques*. Construction & building materials, 2020. **233**: p. 117291.
115. Gao, Y., et al., *Evaluating the effect of corrosion on shear-critical RC beams by integrated NDT*. Developments in the Built Environment, 2021. **7**: p. 100050.
116. Zaki, A., et al., *Monitoring fracture of steel corroded reinforced concrete members under flexure by acoustic emission technique*. Construction & building materials, 2017. **136**: p. 609.
117. Zhang, Y., et al., *Flexural Characteristics Evaluation for Reinforced Concrete Affected by Steel Corrosion Based on an Acoustic Emission Technique*. Applied sciences, 2019. **9**(8): p. 1640.
118. Rodríguez, J., L.M. Ortega, and J. Casal, *Load carrying capacity of concrete structures with corroded reinforcement*. Construction & building materials, 1997. **11**(4): p. 239-248.
119. Nasser, H., et al., *An experimental assessment of corrosion damage and bending capacity reduction of singly reinforced concrete beams subjected to accelerated corrosion*. Construction & building materials, 2021. **286**: p. 122773.
120. ElBatanouny, M.K., et al., *Acoustic emission monitoring for assessment of prestressed concrete beams*. Construction & building materials, 2014. **58**: p. 46-53.
121. Schechinger, B. and T. Vogel, *Acoustic emission for monitoring a reinforced concrete beam subject to four-point-bending*. Construction & building materials, 2007. **21**(3): p. 483-490.
122. Behnia, A., H.K. Chai, and T. Shiotani, *Advanced structural health monitoring of concrete structures with the aid of acoustic emission*. Construction and Building Materials, 2014. **65**: p. 282-302.
123. Webb, G.T., et al., *Analysis of Structural Health Monitoring Data from Hammersmith Flyover*. Journal of Bridge Engineering, 2014. **19**(6): p. 05014003-1 - 05014003-11.
124. Fricker, S. and T. Vogel, *Site installation and testing of a continuous acoustic monitoring*. Construction and Building Materials, 2007. **21**: p. 501-510.
125. Yuyama, S., et al., *Detection and evaluation of failures in high-strength tendon of prestressed concrete bridges by acoustic emission*. Construction and Building Materials, 2007. **21**(3): p. 491-500.

126. Vogel, T., B. Schechinger, and S. Fricker, *Acoustic Emission Analysis as a Monitoring Method for Prestressed Concrete Structures*, in *9th European Conference on NDT (ECNDT)*. 2006: Germany. p. 1-13.
127. Van Steen, C., et al., *Upscaling of acoustic emission monitoring from laboratory experiments to on-site application*, in *Fib CACRCS days 2020 - Capacity Assessment of Corroded Reinforced Concrete Structures*. 2021: Online event. p. 99-106.
128. Faber, M.H., D.V. Val, and M.G. Stewart, *Proof load testing for bridge assessment and upgrading*. *Engineering Structures*, 2000. **22**: p. 1677-1689.
129. Golaski, L., R. Gebiski, and K. Ono, *Diagnostics of reinforced concrete bridges by acoustic emission*. *Journal of Acoustic Emission*, 2002. **20**: p. 83-98.
130. Shiotani, T., D.G. Aggelis, and O. Makishima, *Global Monitoring of Large Concrete Structures Using Acoustic Emission and Ultrasonic Techniques: Case Study*. *Journal of Bridge Engineering*, 2009. **14**(3): p. 188-192.
131. Shiotani, T., D.G. Aggelis, and O. Makishima, *Global monitoring of concrete bridge using acoustic emission*. *Journal of Acoustic Emission*, 2007. **25**: p. 308-315.
132. Yang, Y., D. Hordijk, and A. de Boer. *Acoustic emission study on 50 years old reinforced concrete beams under bending and shear tests*. in *8th international conference on acoustic emission*. 2016.
133. Naik, T.R., V.M. Malhotra, and J.S. Popovics, *The ultrasonic pulse velocity method*, in *Handbook on Nondestructive Testing of Concrete*. 2003, CRC Press. p. 169-188.
134. Takamine, H., et al., *Efficient damage inspection of deteriorated RC bridge deck with rain-induced elastic wave*. *Construction and Building Materials*, 2018. **162**: p. 908-913.
135. Li, W., et al., *Feasibility study of using smart aggregates as embedded acoustic emission sensors for health monitoring of concrete structures*. *Smart Materials and Structures*, 2016. **25**: p. 115031.
136. Song, G., H. Gu, and Y.-L. Mo, *Smart aggregates: multi-functional sensors for concrete structures - a tutorial and a review*. *Smart Materials and Structures*, 2008. **17**: p. 033001.
137. Du, C., Y. Yang, and D.A. Hordijk, *Experimental investigation on crack detection using embedded smart aggregate*, in *Life-Cycle Analysis and Assessment in Civil Engineering: Towards an Integrated Vision*, R. Caspeele, L. Taerwe, and D. Frangopol, Editors. 2018, Taylor and Francis Group: Ghent, Belgium. p. 1199-1206.
138. Lacidogna, G., G. Piana, and A. Carpinteri, *Acoustic Emission and Modal Frequency Variation in Concrete Specimens under Four-Point Bending*. *Applied sciences*, 2017. **7**(4): p. 339.